

RESEARCH ARTICLE

Cranial bone maneuver ameliorates Alzheimer's disease pathology via enhancing meningeal lymphatic drainage function

Xuan Lu^{1,2,3} | Shanshan Bai^{1,2,3} | Lu Feng³ | Xu Yan^{1,2} | Yuejun Lin^{1,2,4} | Junzhe Huang⁵ | Xulin Liao⁶ | Haixing Wang^{1,2,3,4} | Linlong Li³ | Zhengmeng Yang³ | Leo Yik Chun Yan⁵ | Boguang Yang^{1,2,7} | Ming Wang^{1,2} | Jiakang Jin^{1,2} | Zhixian Zong^{1,2} | Zhaowei Jiang^{1,2} | Chuiguo Huang⁸ | Chaoran Liu² | Xiaoting Zhang^{1,2} | Han Su^{1,2,9} | Yaofeng Wang³ | Wayne Yuk-Wai Lee^{1,2} | Xiaohua Jiang¹⁰ | Micky D. Tortorella³ | Sien Lin^{1,2} | Ho Ko⁵ | Gang Li^{1,2,4} 

¹Stem Cells and Regenerative Medicine Laboratory, Li Ka Shing Institute of Health Sciences, The Chinese University of Hong Kong, Prince of Wales Hospital, Hong Kong SAR, PR China

²Musculoskeletal Research Laboratory, Department of Orthopaedics & Traumatology, Faculty of Medicine, The Chinese University of Hong Kong, Prince of Wales Hospital, Hong Kong SAR, PR China

³Centre for Regenerative Medicine and Health, Hong Kong Institute of Science & Innovation, Chinese Academy of Sciences, Hong Kong SAR, PR China

⁴Institute of Biomedicine and Biotechnology, Shenzhen Institute of Advanced Technology, Chinese Academy of Sciences, Shenzhen, PR China

⁵Division of Neurology, Department of Medicine and Therapeutics & Li Ka Shing Institute of Health Sciences, Faculty of Medicine, The Chinese University of Hong Kong, Hong Kong SAR, PR China

⁶Department of Ophthalmology and Visual Sciences, The Chinese University of Hong Kong, Hong Kong SAR, PR China

⁷Department of Biomedical Engineering, The Chinese University of Hong Kong, Hong Kong SAR, PR China

⁸Department of Medicine and Therapeutics, The Chinese University of Hong Kong, Hong Kong SAR, PR China

⁹Department of Neurosurgery, First Hospital of Jilin University, Changchun, PR China

¹⁰MOE Key Laboratory for Regenerative Medicine, School of Biomedical Sciences, Faculty of Medicine, The Chinese University of Hong Kong, Hong Kong SAR, PR China

Correspondence

Gang Li, Stem Cells and Regenerative Medicine Laboratory, Li Ka Shing Institute of Health Sciences, The Chinese University of Hong Kong, Prince of Wales Hospital, Sha Tin, NT, Hong Kong SAR 999077, PR China.
Email: gang.li@siat.ac.cn

Ho Ko, Division of Neurology, Department of Medicine and Therapeutics & Li Ka Shing Institute of Health Sciences, Faculty of Medicine, The Chinese University of Hong Kong

Abstract

INTRODUCTION: Alzheimer's disease (AD) is a progressive neurodegenerative disease and the leading cause of dementia. Recent research highlights meningeal lymphatics as key regulators in neurological diseases, suggesting that enhancing their drainage function could be a potential therapeutic strategy for AD. Our proof-of-concept study demonstrated that cranial bone transport can improve meningeal lymphatic drainage function and promote ischemic stroke recovery.

Xuan Lu and Shanshan Bai have contributed equally to this work.

This is an open access article under the terms of the [Creative Commons Attribution-NonCommercial](https://creativecommons.org/licenses/by-nc/4.0/) License, which permits use, distribution and reproduction in any medium, provided the original work is properly cited and is not used for commercial purposes.

© 2025 The Author(s). *Alzheimer's & Dementia* published by Wiley Periodicals LLC on behalf of Alzheimer's Association.

Kong, Sha Tin, NT, Hong Kong SAR 999077, PR China.

Email: ho.ko@cuhk.edu.hk

Funding information

National Natural Science Foundation of China, Grant/Award Numbers: 82172430, 82272505, 82472454, 81874000, 82122001; University Grants Committee, Research Grants Council of the Hong Kong Special Administrative Region, China, Grant/Award Numbers: 14108720, 14121721, 14202920, 14100122, 14119124, 14113723, N_CUHK472/22, C7030-18G, C6027-19GF, C7074-21GF, T13-402/17-N, AoE/M-402/20, AoE/M-604/16; Health Medical Research Fund (HMRF) of Food and Health Bureau Hong Kong, Grant/Award Numbers: 17180831, 08190416, 09203436; Hong Kong Innovation Technology Commission Funds, Grant/Award Number: PRP/050/19FX; Natural Science Foundation of Guangdong Province, Grant/Award Number: 2023A1515011040

METHODS: This study defined cranial bone maneuver (CBM) technique. After osteotomy, a small circular bone flap was made and attached to an external fixator for subsequent maneuver in a controlled fashion for a defined period using 5xFAD mice.

RESULTS: CBM treatment improved memory functions, reduced amyloid deposits, and promoted meningeal lymphatic drainage function. CBM induced cascades of inflammatory and lymphangiogenic processes in skull and meninges. Meningeal lymphatics are indispensable elements for the therapeutic effects of CBM.

DISCUSSION: CBM might be a promising innovative therapy for AD management, warranting further clinical investigation.

KEYWORDS

Alzheimer's disease, cranial bone maneuver, Interleukin 6, lymphangiogenesis, meningeal lymphatic vessels, vascular endothelial growth factor C

Highlights

- Cranial bone maneuver (CBM) alleviated memory deficits and amyloid depositions.
- CBM promoted meningeal lymphangiogenesis and lymphatic drainage function.
- The beneficial effects of CBM lasted for a long time following the CBM procedures.
- CBM induced cascades of inflammatory and lymphangiogenic processes in the meninges.
- Meningeal lymphatic vessels are indispensable elements for CBM therapeutic effects.

1 | BACKGROUND

Distraction histogenesis (DH) technique has been widely applied in orthopedic surgery for decades.^{1,2} By transforming tension stress stimulation into multiple biological signals, DH technique can significantly boost the regenerative potentials of multiple tissues.³ Derived from DH technique, the cranial bone transport (CBT) technique was used primarily for treating cranial bone deformities and defects. With use of gradual CBT, the continuous stress stimulation during slow bone segment movement promotes angiogenesis, osteogenesis, and tissue regeneration.^{4,5} Clinically, CBT was also found to enhance cerebral circulation and contribute to the regression of neurological deficits in stroke patients.⁶

In recent years, our understanding of the connection between cranial bones and the brain has undergone a radical transformation. Recent investigations employing cutting-edge imaging methods uncovered that many tiny channels in the skull enable the skull bone marrow to be directly exposed to cerebrospinal fluid (CSF), which regulates cell maturation in the skull marrow and inflammatory cell migration into the brain.⁷ Moreover, the skull marrow may reflect inflammatory responses in brain with disease-specific spatial distribution patterns in patients with various neurological disorders.⁸ The meninges, which envelop the brain and spinal cord, play a crucial role in central nervous system (CNS) homeostasis. Meningeal lymphatic vessels (MLVs), which are responsible for the drainage of CSF macromolecules, cellular debris, and immune cells into the deep cervical

lymph nodes (dCLNs), have been characterized in CNS.⁹ The roles of MLVs in different neurological diseases are diverse. Enhancement of meningeal lymphatic drainage has been shown to ameliorate neuroinflammation in subarachnoid hemorrhage, traumatic brain injury, and hepatic encephalopathy,^{10–12} and regulate radiotherapy efficacy through modulating anti-tumor immunity,¹³ whereas meningeal lymphatic dysfunction aggravates the accumulation of amyloid beta (A β) peptides and α -synuclein in brain, contributing to neurodegenerative diseases.^{14,15} In our recent proof-of-concept study, CBT was shown to significantly improve the outcomes of ischemic stroke via enhancing angiogenesis, neurogenesis, and meningeal lymphatic drainage function in the rat middle cerebral artery occlusion model.⁴ These findings underscore a more intricate and intimate relationship between the skull and brain than what we previously understood, and further provide a rationale for potentially treating neurological diseases via maneuvering the cranial bone, while the potential mechanisms have yet to be fully elucidated.

Alzheimer's disease (AD) is a progressive neurodegenerative disease and the most common cause of dementia, resulting in a deterioration of mood, cognition, and memory.¹⁶ Due to the increasing aging population, approximately 50 million people have AD globally,¹⁷ which imposes a tremendous socioeconomic burden on the health care system. AD is a heterogenous disease, with several cognitive subtypes and varying biological and clinical manifestations.^{18,19} It has been reported that amyloid immunotherapy may induce microhemorrhages and neuronal disturbances, and worsen iron deposits in the

CNS in patients with AD.^{20–22} As a result, there is a growing need for more controllable and effective approaches for AD management. In this study, we tested the therapeutic potential of cranial bone maneuver (CBM) technique in AD transgenic mouse model and explored the underlying mechanisms.

2 | METHODS

2.1 | Animals

Adult male 5xFAD (B6SJL) transgenic mice (Tg6799, The Jackson Laboratory, RRID: MMRRC_034840-JAX) were used in this study. The hemizygous 5xFAD mice overexpress human A β precursor protein 695 with the Swedish (K670N, M671L), Florida (I716 V), and London (V717I) mutations together with human presenilin 1 harboring the M146L and L286 V mutations under the control of the mouse Thy1 promoter element. Age-matched non-transgenic littermates were included as wild-type (WT) controls. Adult and senescent C57BL/6 mice were used to investigate the effects of aging on meningeal lymphatics. All mice were housed in the Laboratory Animal Research Centre of the Chinese University of Hong Kong, in a controlled environment with a 12 h light/dark cycle, a constant room temperature ($23 \pm 1^\circ\text{C}$), and unrestricted access to food and water. All surgeries were performed under anesthesia, and efforts were made to minimize the suffering of the animals. All animal experiments were carried out in Li Ka Shing Institute of Health Sciences, Prince of Wales Hospital, with the approval of the Department of Health of the Government of Hong Kong and the Chinese University of Hong Kong Animal Experimentation Ethics Committee (No. 21-001-MIS).

2.2 | CBM surgery

A custom-made external fixator device was used for CBM procedures. 5xFAD mice were anesthetized with ketamine (80–100 mg/kg) and xylazine (10 mg/kg) in normal saline and then placed in a prone position with the head skin shaved and sterilized. The head of the mouse was secured in a stereotaxic frame (RWD life sciences, Shenzhen, China). Mice head skin was incised with a ≈ 1.5 cm length. A circular bone flap (diameter of ≈ 2 mm) was created using a small drill cutter with careful protection of the dura. The cranial flap site was irrigated with normal saline. Two additional holes were drilled on the intact skull to secure the external fixator, and one screw was attached to the bone flap (Figure 1A and Figure S1). The skin incision was closed with 5-0 nylon sutures. After 3 days of latency, the bone flap underwent a sequential displacement procedure. This involved an initial upward movement on the first day (day 1), followed by a subsequent downward repositioning the next day (day 2). This alternating pattern of up and down movements was repeated for a total of 10 days. Each adjustment was made by delicately manipulating the screw on the device, allowing for a controlled vertical displacement at a rate of 0.1 mm/day (Figure 1A,B). For the CBM control group (abbreviated as CBM Ctrl in Figures), mice

RESEARCH IN CONTEXT

- 1. Systematic review:** Alzheimer's disease (AD) is a progressive neurodegenerative disease and the most common cause of dementia. There is no effective therapy that halts AD progression at present. Meningeal lymphatics have recently been recognized as an important regulator in neurological diseases. The augmentation of meningeal lymphatic drainage function might be a promising therapeutic approach for AD. Our previous study showed that cranial bone transport can modulate meningeal lymphatic drainage function and promote ischemic stroke recovery.
- 2. Interpretation:** We defined the CBM technique. CBM treatment significantly improved memory functions, reduced amyloid deposits, and increased meningeal lymphatic vessels (MLVs) using 5xFAD mice. CBM induced cascades of inflammatory responses and lymphangiogenic processes in the meninges. MLVs are indispensable elements for CBM therapeutic effects.
- 3. Future directions:** CBM might be a novel promising approach for AD management by augmenting the meningeal lymphatic drainage function. Further clinical investigations are highly warranted.

received craniectomy, which was fixed with the same external device, but CBM procedure (up and down displacement) was not applied. Buprenorphine HCl (0.05 mg/kg) was subcutaneously administered 30 min before surgery, and a heating pad was provided after surgery to maintain body temperature during surgery and recovery. Buprenorphine HCl (0.05 mg/kg) was subcutaneously administered twice daily for 5 consecutive days after surgery for pain and stress relief. The mice were free to move in the cages. Body temperature, body weight, food and water intake, and the conditions of surgical incision were checked daily in the whole experimental duration.

2.3 | Behavior tests

Animals were habituated to the testing environment for 10 days (15 min per day) before behavioral tests. The room temperature ($23 \pm 1^\circ\text{C}$) and humidity ($60 \pm 10\%$) remained stable for all experiments. Animals were randomly assigned to test groups and the researchers were blinded to animal assignments.

2.3.1 | Open field test

The open field test was used to assess locomotor activity and anxiety in mice. Each mouse was placed in the center of an opaque chamber (35 cm \times 35 cm \times 25 cm) and allowed to freely explore in the arena for

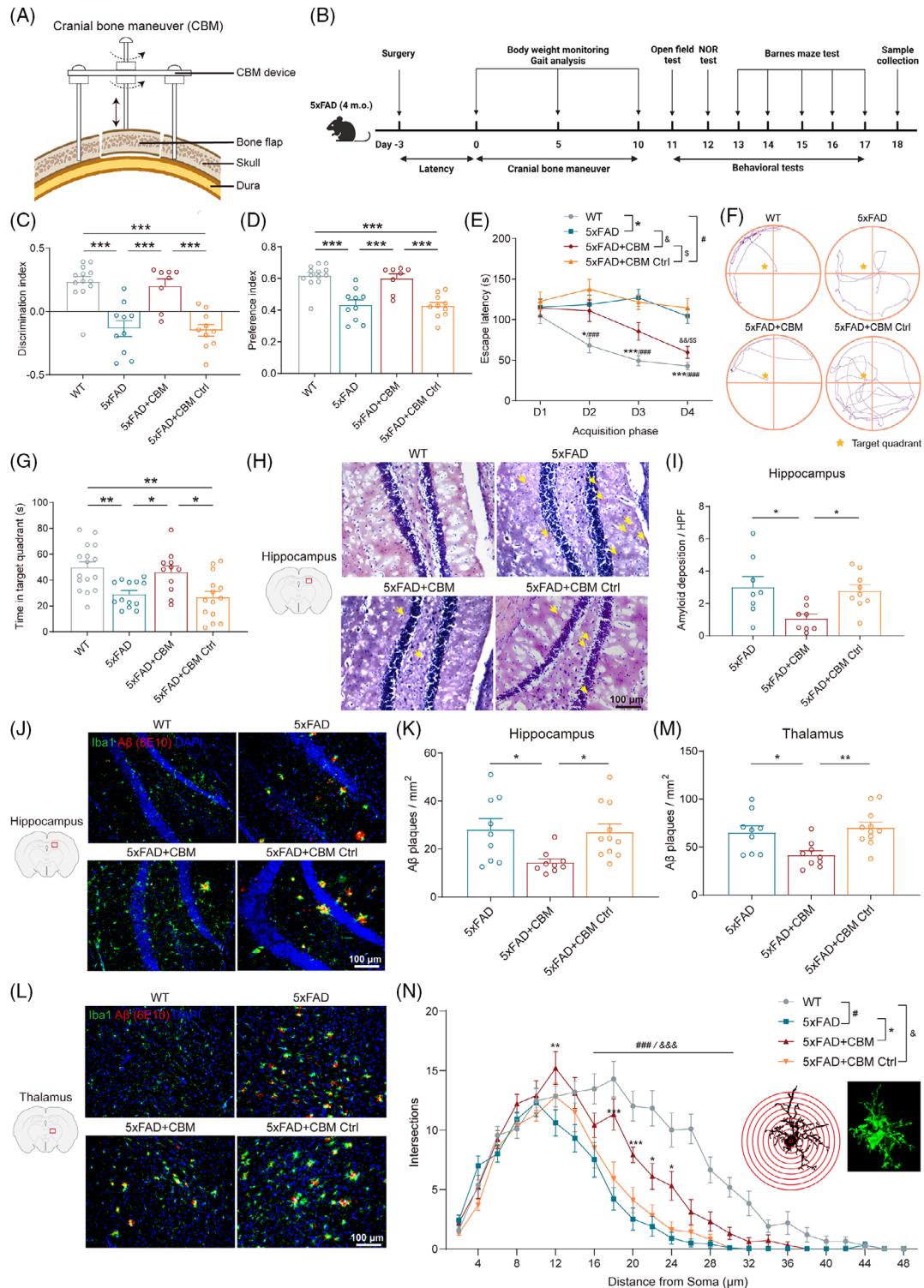


FIGURE 1 CBM improved memory function, reduced amyloid depositions and A β plaques, and alleviated neuroinflammation of 5xFAD mice. (A) A schematic diagram of CBM. (B) Experimental timeline for the CBM treatment and behavioral tests. (C and D) For NOR test, the discrimination index, and preference index were significantly increased in 5xFAD mice treated with CBM, compared with 5xFAD and 5xFAD+CBM Ctrl group. $n = 8-13$ mice/group. (E-G) In Barnes maze test, CBM significantly improved the spatial memory functions of 5xFAD mice, with the escape latency significantly decreased (E) and the time spent in target quadrant significantly increased (F and G), $n = 11-16$ mice/group. CBM significantly reduced amyloid depositions (as yellow arrows indicated, H and I) in hippocampus and A β plaques (J-M) in both the hippocampus and thalamus of 5xFAD mice; $n = 8-11$ mice/group. (N) Sholl analysis indicated that neuroinflammation of 5xFAD mice was significantly alleviated after the treatment of CBM (representative images of Iba1 staining and Sholl analysis were shown); $n = 5$ mice/group. Values are means \pm SEM. */&/\$/# $p < 0.05$, **/&&/&/\$ $p < 0.01$, and ***/###/&&& $p < 0.001$, one-way or two-way ANOVA with Bonferroni's post hoc tests among groups. CBM, cranial bone maneuver; HPF, high-power field; NOR, novel object recognition; SEM, standard error of the mean.

10 min. Spontaneous locomotor activity was recorded by an automated video tracking system. A smaller concentric square covering 25% of the area (17.5 cm × 17.5 cm) was defined as the central area. The locomotion parameters including time in the center and total distance in the entire zone were analyzed by ANY-maze software (version 4.98, Stoelting Co. Wood Dale, IL).

2.3.2 | Novel object recognition test

The novel object recognition (NOR) test was performed following a published protocol with modifications.²³ The experimental setup consisted of a square box identical to the one utilized in the open field test. The experiment included three trials with a 2-h training-to-testing interval: (1) A habituation trial: a 10-min session in the empty apparatus; (2) A training (familiarization) trial: a 10-min session presenting two identical objects located 15 cm apart; and (3) A testing trial: each mouse was returned to the apparatus for a 10-min session in which one of the objects was replaced by a novel one (different color and shape). Mouse behavior was recorded and analyzed by an investigator who was blinded to the treatment group. Exploration of an object was assumed when the mouse approached an object and touched it with its vibrissae, snout, or forepaws and was analyzed using ANY-maze software (version 4.98, Stoelting Co. Wood Dale, IL). Discrimination index ($[\text{time spent with novel object} - \text{time spent with old object}] / \text{total exploration time}$) and preference index ($\text{time spent with novel object} / \text{total exploration time}$) were calculated.

2.3.3 | Barnes maze test

Barnes maze test was conducted for successive 5 days following a published protocol with modifications.²⁴ Visual cues with different colors and shapes were prepared and strategically placed surrounding the maze. Each mouse was placed in a cylindrical black start chamber in the center of the maze. All mice underwent four trials per day during the acquisition phase (4 days). Prior to the commencement of each trial, the maze was thoroughly cleaned with a 1% Incidin solution to eliminate any potential olfactory cues affecting the results. In addition to cleaning, the maze was rotated around its central axis after each trial to control for possibly remaining odor cues. Each mouse was given 180 s to locate the escape hole in different quadrants for each trial. If the mouse found the escape hole before the 180 s cutoff time, mice were allowed to stay in the box under the escape hole for 60 s and then return to home cage. If failed, mice were guided to rest in the box under escape hole for 60 s before being assisted back into the home cage, and the latency was recorded as 180 s. Mice were trained in each quadrant with an interval of 15 min between two trails. On the fifth day, the probe test was conducted 24 h after the last training. The escape hole was closed, and each mouse was placed into the center of the maze under the cylindrical black start chamber. The movement track, the crossing numbers of target quadrant, and the percentage of time staying in the target quadrant within a 90 s trial time was recorded and

analyzed using ANY-maze software (version 4.98, Stoelting Co. Wood Dale, IL).

2.3.4 | Catwalk gait analysis

Automated gait analysis was performed during CBM procedures using a CatWalk system (Noldus, Wageningen, Netherlands) as described previously.²⁵ A green light below the glass walkway illuminated the paws of mice as they walked across it, and their movements were recorded by a high-speed video camera. The camera settings were adjusted with an intensity threshold of 0.12, a gain of 31, and a maximum allowed speed variation of 60%. All experiments were conducted in the same environment by the same investigator. Three trials of walking were recorded for each mouse and the computer recorded parameters of the right front (RF) paw, right hind (RH) paw, left front (LF) paw, and left hind (LH) paw of all mice, including maximum paw print intensity and stride length. Gait analysis was performed on days 0, 5, and 10 during the CBM procedures.

2.4 | Intra-cisterna magna injection

Mice were anesthetized by intraperitoneal injection of a mixed solution of ketamine (80–100 mg/kg) and xylazine (10 mg/kg) in saline. The head of the mouse was secured in a stereotaxic frame (RWD life sciences, Shenzhen, China). The skin of the neck was shaved and sterilized. After an incision (≈ 1 cm) was made, the muscle layers were retracted, and the cisterna magna was located. For meningeal lymphatic drainage experiments, intra-cisterna magna (I.C.M) injection was conducted for mice that completed all designed behavioral tests. Using a Hamilton syringe with a 33G needle, 5 μL of ovalbumin conjugated with Alexa Flour 647 (OVA-A647, O34784, Thermo Fisher Scientific, USA) at a concentration of 0.5 mg/mL in artificial CSF (597316, Harvard Apparatus, UK) was injected into the cisterna magna with a rate of 2.5 $\mu\text{L} / \text{min}$. The syringe was left in place for an additional 2 min to prevent backflow of CSF after injection. The neck skin was then sutured, and the mouse was allowed to recover on a heat pad until fully awake.

2.5 | MLVs ablation

Visudyne treatment was conducted according to previous studies.²⁶ In brief, mice were anesthetized with ketamine (80–100 mg/kg) and xylazine (10 mg/kg) in normal saline and the mouse head was fixed in a stereotaxic instrument (RWD life sciences, Shenzhen, China). Visudyne (verteporfin for injection, Valeant Ophthalmics, USA) was reconstituted at 2 mg/mL according to the manufacturer's instructions, and 5 μL of Visudyne was injected into the cisterna magna at a speed of 2.5 $\mu\text{L} / \text{min}$. Fifteen min later, a nonthermal 689-nm wavelength laser light (Ningbo Yuanming Laser Technology, China), with a dose of 50 J / cm^2 and intensity of 600 mW / cm^2 , was applied on five different spots through the skull (two on the transverse sinus, two

on the superior sagittal sinus, and the injection site), and each spot was irradiated for 83 s. For the Vehicle+Laser group, mice underwent the same procedures of vehicle injection and laser treatment without Visudyne. During the laser treatment, the eyes of the mice were cover-protected. The skin was then sutured with 5-0 nylon sutures, after which the mice were allowed to recover on a heat pad until fully awake. After surgery, mice were given analgesics subcutaneously. For the CBM group, mice underwent the same CBM surgical procedures as aforementioned 7 days after the Visudyne/Vehicle+Laser treatment.

2.6 | Osmotic pump I.C.M long-term infusion

MAZ51 in dimethyl sulfoxide (Cat. No. HY-116624, MedChemExpress, USA) was dissolved in 20% SBE- β -CD (Sulfobutylether- β -Cyclodextrin, Cat. No. HY-17031, MedChemExpress, USA) in artificial CSF (597316, Harvard Apparatus, UK) at 0.1 mM and loaded into the capsule of osmotic pump (1004 W, RWD life sciences, Shenzhen, China) with a total volume of 100 μ L. The osmotic pumps were connected to a 33G needle with a limited length of 1.5 mm and incubated overnight in a 37°C water bath. The tiny needle of osmotic pump was inserted into and fixed at the cisterna magna, whereas the pump was placed subcutaneously, which can achieve continuous I.C.M infusion at a rate of 0.125 μ L/h for 4 weeks. The vehicle group was given the same volume of vehicles. The skin was sutured by 5-0 nylon sutures, and mice received postsurgical buprenorphine HCl. For the CBM treatment group, mice underwent the same CBM surgical procedures as aforementioned 7 days after the osmotic pump implantation.

2.7 | Tissue preparation

Mice were anesthetized and transcardially perfused with 50 mL of ice-cold sterile normal saline. Skulls were carefully removed and fixed in 4% paraformaldehyde (PFA, Sigma-Aldrich, P1468) overnight at 4°C. The skulls were then decalcified in 10% ethylenediaminetetraacetic acid (EDTA) for 28 days for further histological analysis. Brains and dCLNs were fixed in 4% PFA overnight at 4°C, followed by sequentially transferring to 10%, 20%, and 30% sucrose solution at 4°C for 72 h. Samples were embedded in optimal cutting temperature compound (OCT, Sakura Finetek, USA). Coronal brain, skull, and dCLNs sections in 15- μ m thickness were obtained using a freezing microtome (NX70, Thermo Scientific).

2.8 | Congo red staining

The brain sections were first immersed in distilled water for 15 min and then placed in 0.3% Congo red working solution for another 15 min.²⁷ Subsequently, the sections were rinsed with distilled water and quickly

differentiated into an alkaline alcohol solution for 3 s. After that, the sections were washed with tap water for 1 min and counterstained with hematoxylin solution for 3 min. Following this, they were washed again with running tap water for 1 min and rinsed with acid alcohol for 1 s. The sections were then rinsed with Scott's tap water for 3 min and dehydrated using 95% and 100% alcohol. Finally, the sections were cleared with xylene and mounted using dibutylphthalate polystyrene xylene (DPX) mounting medium.

2.9 | Immunofluorescence staining

The fresh-frozen brain sections were fixed with 4% PFA for 15 min and then rinsed and washed three times with 1 \times phosphate-buffered saline (PBS) for 5 min each time. Subsequently, the sections were incubated in 0.5% Triton X-100 for 15 min and blocked with 2% donkey/goat serum and 5% bovine serum albumin (BSA, SRE0098, Sigma-Aldrich, USA) for 2 h at room temperature. After the blocking step, the sections were incubated overnight at 4°C with the appropriate dilutions of primary antibodies (Table S1). The sections were then washed eight times with 1 \times phosphate buffered saline with 0.1% Tween 20 (PBST) for 5 min each time and incubated with secondary antibodies for 1 h at room temperature in the dark (Table S1). After washed eight times with 1 \times PBST for 5 min each time, the sections were incubated with 4',6-diamidino-2-phenylindole (DAPI) to label the cell nucleus, and were subsequently mounted using proLong Gold Antifade Mountant (P36934, Thermo Fisher Scientific).

2.10 | Immunohistochemistry staining

The coronal skull sections were fixed with 4% PFA for 15 min and then rinsed and washed three times with 1 \times PBS for 5 min each time. Antigen retrieval was performed by rinsing sections into a boiled 1 \times citrate buffer (pH 6.0, G1202, Wuhan Servicebio Technology Co., Ltd.), and incubating at 95°C for 20 min, followed by 1 h cooling at room temperature. Endogenous peroxidase activity was quenched by treating samples with 3% H₂O₂ for 10 min at room temperature. Sections were blocked in 10% BSA for 2 h, and then were incubated with the appropriate dilutions of primary antibodies (Table S1) overnight at 4°C. The sections were washed eight times with PBST for 5 min each time, before addition of horseradish peroxidase (HRP)-conjugated secondary antibody for 30 min incubation at room temperature. Sections were washed eight times with PBST after secondary incubation and 3,3'-diaminobenzidine (DAB) substrate was then added until positive signal was observed (PV-9000, ZSGB-BIO). The sections were washed with tap water for 1 min and counterstained with hematoxylin solution for 3 min. Following this, they were washed again with running tap water for 1 min and rinsed with acid alcohol for 1 s. The sections were then rinsed with Scott's tap water for 3 min and dehydrated using 95% and 100% alcohol. Finally, the sections were cleared with xylene and mounted using DPX mounting medium.

2.11 | Whole mount staining

The mouse skull together with meninges was fixed in 4% PFA for 24 hours at 4°C. Using a fine forceps, the meninges were gently detached and removed from the skull along the superior sagittal sinus and transverse sinus under a stereo microscope (SZ SERIES, OPTIKA S.r.l. Italy). It is important to remove any small pieces of skull bone attached to the meninges.²⁸ The meninges were then permeabilized with 0.5% Triton X-100 for 1 h and incubated in PBS containing 2% donkey serum and 5% BSA at room temperature for 2 h. Incubation with primary antibodies (Table S1) was performed overnight at 4°C. The meninges were washed eight times for 10 min each time with PBST, and then rinsed in the appropriate secondary antibody for 2 h at room temperature (Table S1). After being washed with PBST and labeled with DAPI, the meninges were mounted using proLong Gold Antifade Mountant (P36934, Thermo Fisher Scientific).

2.12 | Image analysis

Microscopic imaging system (Leica DM5500; Leica Microsystems, Wetzlar, Germany) was used to acquire images. ImageJ software (National Institutes of Health [NIH], USA) was used for quantitative measurements. Three inconsecutive sections from each brain were selected randomly for quantitative analyses. The number of positive amyloid depositions by Congo red staining in the region of interest (ROI) of different brain regions (cortex, hippocampus, and thalamus) was counted by an investigator who was blinded to group assignment to determine the density of amyloid depositions in different brain regions. For immunofluorescence staining, the number and area of positive A β (6E10) plaques in the ROI of different brain regions (cortex, hippocampus, and thalamus) were measured by an investigator who was blinded to group assignment to determine the density and size of A β plaques using the automatic threshold tool in ImageJ. To assess the microglial engulfment of A β , we quantitatively measured the area exhibiting dual positive staining for Iba1 and A β (6E10). This area was subsequently normalized by the total area of A β (6E10) staining within the same ROI. The meningeal lymphatic drainage function was evaluated by the area fraction of OVA-A647⁺ area in dCLNs sections. For whole mount staining, the area fraction of LYVE1⁺ or CD31⁺ area in the ROI was used to determine the quantification of meningeal lymphatic and blood vessels. All images were evaluated by an investigator who was blinded to the group assignment.

2.13 | Sholl analysis

To perform Sholl analysis, serially stacked and maximally projected images were obtained using a confocal microscope (LSM 880 Confocal Laser Scanning Microscope, Zeiss, Germany) under 63 \times objectives.²⁶ Brain section images that were immunofluorescence stained with Iba1 antibody were used for Sholl analysis. Two fields of view in the peri-A β

area of the thalamus region were imaged for each section, and two sections were imaged for each mouse. Four microglia per field of view were quantified for five mice per group. The Sholl analysis plugin applied in ImageJ (NIH, USA) constructed serially concentric circles at 2 μ m intervals from the center of the Iba1 signal (soma) to the end of the most distal process of each microglia. The number of intersections of Iba1-positive processes at each circle and the radius of the largest circle intercepting the microglia were analyzed. All analyses were performed blindly to group assignments.

2.14 | RNA-sequencing analysis

Mice were anesthetized and transcardially perfused with 50 mL of ice-cold sterile diethyl pyrocarbonate (DEPC)-treated normal saline. The skulls and meninges were carefully removed, detached, and immediately snap-frozen in liquid nitrogen and stored at -80°C for extraction of RNA. The transcriptomic analysis included five mice in each group. Meninges RNA was isolated using RNeasy micro kit (QIAGEN, 74004, USA), and DNA was removed using DNase I digestion, following the manufacturer's instructions.²⁹ RNA samples with the RNA integrity number (RIN) values >7.0 were used for downstream library construction. RNA sequencing libraries were constructed using the DNBseq platform (BGI, China). The raw data were filtered to obtain the clean data, which were used for alignment to the mouse genome (*Mus musculus* GRCm38.p5, NCBI). Statistical significance of differentially expressed genes (DEGs) was obtained based on the raw read counts, with an absolute log₂ fold-change greater than 1, and adjusted *p*-value (*q*-value) less than 0.05. Gene ontology (GO), Kyoto Encyclopedia of Genes and Genomes (KEGG) and tissue enrichment analysis was performed using DAVID (<https://david.ncifcrf.gov>).^{30,31} The gene expression heatmap was drawn with Heatmapper.³² The protein-protein interaction network was drawn with Cytoscape (Version 3.10.0, Cytoscape Consortium, USA). The results were visualized by the R package ggplot2 (Version 3.6.3, R software).

2.15 | Cell culture

The murine-derived macrophage cell line RAW264.7 was maintained in Dulbecco's Modified Eagle Medium (DMEM, Gibco, Thermo Fisher Scientific) supplemented with 10% fetal bovine serum (FBS, ExCell Bio, FSP500) and 1% penicillin/streptomycin (Gibco, Thermo Fisher Scientific). Human dermal lymphatic endothelial cells (LECs, #2010, ScienCell Research Laboratories, Inc.) were cultured in endothelial cell basal medium-2 (EGM-2MV BulletKit medium, CC-3162, Lonza, USA) supplemented with growth factors (5% FBS, vascular endothelial growth factor [VEGF], fibroblast growth factors [FGF], epidermal growth factor [EGF], and insulin-like growth factor [IGF]) and were seeded on Attachment Factor Protein (S006100, Gibco, Thermo Fisher Scientific) coated wells and flasks. The cells were cultured at 37°C in a humidified incubator with 5% CO₂.

2.16 | In vitro cellular mechanical stretch

To apply lineal mechanical stretch onto macrophages, RAW264.7 cells were uniformly seeded into a collagen I-coated culture chamber with flexible silicon membrane bottoms (Cell & Force, Hangzhou, China). CELL TANK stretching system (Cell & Force, Hangzhou, China) was used to apply lineal continuous tensile strain onto RAW264.7 cells for 24 h and 48 h. Cells that were cultivated in the same chambers with same culture medium but were not stretched are used as control group. After completion of mechanical stretch, total RNA in RAW264.7 cells was extracted using RNAiso Plus reagent (TaKaRa, Japan) following the manufacturer's instructions.

2.17 | In vitro assays of human dermal LECs

2.17.1 | Proliferation assay

Proliferation assays were performed using the Cell Counting Kit-8 (CCK-8, C0037, Beyotime, China) according to the manufacturer's instructions. All experiments were performed on 96-well plates with four replicates. Briefly, human dermal LECs were diluted to 1×10^4 cells/mL in EGM-2MV (Lonza, USA), and 0.2 mL of cells were added to each well. Plates were cultured at 37°C/5% CO₂ for 24 h. Plates were washed with PBS once and then serum starved in EBM-2 basal medium (Lonza, USA) containing 0.5% FBS for 12 h. Recombinant human interleukin 6 (IL-6) protein (206-IL-025/CF, R&D Systems, Inc.) and vehicle were added to cells and incubated for 24 and 48 h. Cell proliferation was measured by following the addition of CCK-8 (0.02 mL) to each well and incubation for a further 4 h. Absorbance was measured at 450 nm on VICTOR X4 Multimode Plate Reader (Perkin Elmer, USA).

2.17.2 | Tube-formation assay

Tube-formation assays were performed using GelTrex (A14132-02, ThermoFisher Scientific). GelTrex was thawed on ice and wells of a 48-well plate were coated with 100 µL GelTrex matrix and heated to 37°C for 30 min to allow the GelTrex to solidify. Then 5×10^4 cells were added per well with the treatment of recombinant human IL-6 protein (20 ng/mL, 206-IL-025/CF, R&D Systems, Inc.), Tocilizumab (100 ng/mL, Anti-Human IL-6R, Humanized Antibody, HY-P9917, MedChemExpress), or vehicle, and were incubated for 16 h at 37°C with 5% CO₂. Images of sprouts were captured using an inverted phase contrast microscope (Axiovert 5, ZEISS), and the number of branches and total length were quantified using "Angiogenesis Analyzer" plugin³³ of ImageJ Fiji software (NIH, USA). All images were evaluated by an investigator who was blinded to the group assignment.

2.17.3 | Migration scratch assay

All experiments were performed in pre-marked 12-well plates with four replicates. Human dermal LECs were diluted to 1×10^5 cells/mL

and 2 mL of cells was added to each well. Cells were cultured in EGM-2MV (Lonza, USA) at 37°C/5% CO₂ until confluent. Cells were then starved in EBM-2 basal medium (Lonza, USA) containing 0.5% FBS for 12 h. A single scratch was made in each confluent cell layer using a 200 µL pipette tip, and cells were washed gently in EBM-2 basal medium (Lonza, USA). Images at time 0 (initial) were captured using an inverted phase contrast microscope (Axiovert 5, ZEISS). Cells were then incubated in EBM-2 basal medium containing the treatment of recombinant human IL-6 protein (20 ng/mL, 206-IL-025/CF, R&D Systems, Inc.), Tocilizumab (100 ng/mL, Anti-Human IL-6R, Humanized Antibody, HY-P9917, MedChemExpress), or vehicle. Images were captured 12 and 24 h later. Scratch areas were measured using ImageJ software (NIH). Wound closure percentage was calculated for further analysis. All images were evaluated by an investigator who was blinded to the group assignment.

2.18 | RNA isolation and RT-qPCR

5xFAD mice skull were dissected into pieces. Total RNA in 5xFAD mice skulls, RAW264.7 cells, or human dermal LECs were extracted using RNAiso Plus reagent (TaKaRa, Japan) following the manufacturer's instructions. RNA was translated reversely into complementary DNA (cDNA) with a PrimeScript RT Master Mix (RR036A, Takara, Japan). RT-qPCR (Real-time quantitative polymerase chain reaction) was performed in ABI QuantStudio7 (Applied Biosystems) using PowerUp SYBR Green Master Mix (A25776, Thermo Fisher Scientific). The 10-µL reaction system contained 5 µL of SYBR Green Master Mix, 0.5 µL of forward and reverse primers, 1 µL of target cDNA, and supplemented with nuclease-free H₂O. The relative gene expression was quantified using the 2^{-ΔΔCt} method. The messenger RNA (mRNA) expression levels were normalized with glyceraldehyde-3-phosphate dehydrogenase (GAPDH). Table S2 displays the details of primers.

2.19 | Enzyme-linked immunosorbent assay

Mice were anesthetized and transcardially perfused with 50 mL of ice-cold sterile normal saline. The skulls and meninges were carefully removed, detached, and immediately snap-frozen in liquid nitrogen and stored at -80°C for extraction of proteins. The skulls and meninges were lysed in radioimmunoprecipitation assay (RIPA) buffer supplemented with 1 mM phenylmethylsulfonyl fluorid (PMSF), and protease inhibitor cocktail (Solarbio Life Science, China). The supernatant was collected after centrifugation at 12,000× g for 10 min at 4°C. The total protein concentration of each sample was detected using Pierce BCA Protein Assay Kits (23227, Thermo Fisher). The protein levels of VEGF-C (RK04299, ABclonal), VEGF-D (NBP2-78891, Novus Biologicals), IL-1β (MLB00C, R&D Systems), IL-6 (M6000B-1, R&D Systems), IL-10 (JL20242, JONLNBIO), and TGF-β (transforming growth factor-β, JL13959, JONLNBIO), were detected using commercially available enzyme-linked immunosorbent assay (ELISA) kits according to the manufacturer's instructions. Standard curves were constructed based

on the absorbance of corresponding standard solutions using VICTOR X4 Multimode Plate Reader (Perkin Elmer, USA) at 450 nm. The concentration of each experimental sample was obtained by fitting the absorbance value into the standard curves.

2.20 | Statistical analysis

Statistical analysis was performed using GraphPad Prism (Version 8.0.1, CA, USA). Data are presented as mean \pm standard error of the mean (SEM). Normal distribution of data was first checked with the Anderson-Darling, D'Agostino, and Shapiro-Wilk normality tests. Student's *t*-tests (two-tailed) were used to compare means between two groups with normally distributed data. One-way or two-way analysis of variance (ANOVA) with Bonferroni's post hoc tests were used for multiple comparisons among three or more groups. Each *n* indicates the number of biologically independent replicates. No statistical methods were used to predetermine sample size. Sample sizes were chosen based on previous experiments. *p*-value less than 0.05 was considered statistically significant.

2.21 | Data and materials availability

The key data supporting the findings of this study are presented within the article and the [Supplementary Information](#).

3 | RESULTS

3.1 | The therapeutic effects of CBM on AD progression

First, we aimed to examine whether CBM could modulate AD pathology progression. Briefly, a circular cranial bone flap was created with careful protection of the dura. Two additional holes were drilled on the intact skull to secure the external fixator, and one screw was attached to the bone flap (Figure 1A and Figure S1). We performed CBM procedures (upward and downward bone flap movement) on 4-month-old (4 m.o.) 5xFAD mice for 10 days, after a latency of 3 days following CBM surgery (Figure 1B, details can be found in Methods 2.2). In the NOR test, the discrimination index (Figure 1C) and preference index (Figure 1D) were significantly decreased in 5xFAD mice group, compared with the WT group. CBM significantly improved nonspatial memory function of 5xFAD mice, but no significant changes were observed in the CBM control group. In the Barnes maze test, the escape latency was significantly decreased in the 5xFAD mice treated with CBM during the acquisition phase (Figure 1E). During the probe test phase, no significant difference of total travel distance was detected in the groups (Figure S2A), whereas 5xFAD mice treated with CBM spent more time in the target quadrant (Figure 1F,G). These data indicated that the memory function of 5xFAD mice was significantly improved after the treatment of CBM.

To evaluate the well-being and motor function of 5xFAD mice, body weight monitoring and gait analysis were performed during the CBM procedures, and the open field test was conducted after the CBM treatment. No significant changes of body weight (Figure S2B), maximum paw intensity (Figure S2C,D), or stride length (Figure S2E,F) were detected among the groups throughout the CBM procedures. The open field test showed no significant difference in terms of total travel distance (Figure S2G), entries of central zone (Figure S2H), or time spent in the central zone (Figure S2I,J) among groups after the treatment of CBM. Collectively, these findings suggested that CBM surgery did not affect the body weight and motor function of 5xFAD mice; neither did CBM induce anxiety in 5xFAD mice.

Histopathological examination revealed that the density of amyloid depositions (Congo red staining) was significantly decreased in the hippocampus (Figure 1H,I), but not in the cortex or the thalamus of 5xFAD mice treated with CBM (Figure S3A–D). Similarly, CBM treatment significantly reduced the density of A β plaques (quantified based on 6E10 antibody staining) in the hippocampus and thalamus (Figure 1J–M), but not the cortex of 5xFAD mice treated with CBM (Figure S3E,F), whereas no significant difference was detected for the average A β plaque size across the groups (Figure S3G–I). Sholl analysis of microglia morphology demonstrated that neuroinflammation was alleviated by CBM, as evidenced by the increased ramification of microglia in the thalamus (Figure 1N). However, the co-localized area percentage of A β plaques (6E10) and microglia (Iba1⁺) were not affected by CBM treatment (Figure S3J–L).

3.2 | CBM promoted meningeal lymphangiogenesis and meningeal lymphatic drainage function in 5xFAD mice

Previous studies have suggested that aging can lead to the reduction of MLVs,^{15,34} and AD can further deteriorate impairment.³⁵ In this study, we harvested the meninges of C57BL/6 mice at the ages of 4 and 24 months old (m.o.). In 24 m.o. mice, the MLVs in the superior sagittal sinus, transverse sinus, and confluence of sinus were all significantly decreased, compared with 4 m.o. mice (Figure S4A–E). In addition, a premature decrease of MLVs in the superior sagittal sinus and transverse sinus (Figure S4F–H), but not confluence of sinus (Figure S4I), was observed in 12 m.o. 5xFAD mice compared to 12 m.o. WT counterparts. Collectively, these data showed that aging impairs the structural integrity of MLVs, which is further accentuated by AD pathology.

Brain health is closely linked to fluid flow dynamics that remove potentially harmful waste. The meningeal lymphatic drainage function was found to play an important role in this process.^{36,37} We investigated the effects of CBM on meningeal vasculature and lymphatic vessels, by examining the meninges isolated from mouse skull. We used CD31 and LYVE-1 to label meningeal blood vessels (CD31⁺ and LYVE-1⁻) and MLVs (LYVE-1⁺) and studied their changes after CBM treatment (Figure S5). A significant increase of LYVE-1⁺ area fraction of MLVs in the superior sagittal sinus and transverse sinus, but not in the confluence of sinus, was observed in 5xFAD mice treated with

CBM (Figure 2A-I), indicating that CBM could promote meningeal lymphangiogenesis. However, no significant changes in meningeal blood vessels were detected in those regions (Figure 2C, F, and I). To further investigate the effects of CBM on the drainage function of MLVs, OVA-A647 was I.C.M injected (Figure 2J). No significant difference in the area fraction of OVA-A647 in meninges was detected among groups (Figure S6A,B). The area fraction of OVA-A647 in dCLNs was significantly increased 3 h after I.C.M injection in 5xFAD mice treated with CBM (Figure 2K,L). Collectively, these results suggested that the therapeutic effects of CBM in the 5xFAD mouse model are closely associated with the promotion of meningeal lymphangiogenesis and the enhancement of meningeal lymphatic drainage function.

3.3 | The long-term therapeutic effects of CBM on AD

We then investigated the long-term effects of CBM on AD progression. This was carried out by conducting the CBM procedures for 10 days in 5xFAD mice, and the external device was removed upon the completion of CBM procedures. The locomotion activities and memory functions of the 5xFAD mice were evaluated 60 days after the CBM procedures (Figure 3A) when the mice were 6 m.o. (hereafter referred to as 5xFAD [6 m.o.]). In the open field test, no significant differences in total travel distance, entries of central zone, or time spent in the central zone were observed between two groups after CBM (Figure S7A-C). In the NOR test, the discrimination index (Figure 3B) and preference index (Figure 3C) were significantly improved in 5xFAD (6 m.o.) mice treated with CBM, compared with non-treatment group. In the Barnes maze test, the escape latency was significantly decreased in 5xFAD (6 m.o.) mice treated with CBM during the acquisition phase (Figure 3D). During the probe test phase, no significant difference in total travel distance was detected between the two groups (Figure S7D), whereas 5xFAD (6 m.o.) mice treated with CBM spent more time in the target quadrant (Figure 3E,F). In summary, these results showed that the memory functions of 5xFAD (6 m.o.) mice can be improved significantly with long-lasting effects after CBM treatment.

Histopathological results revealed significant reductions of amyloidosis in the thalamus of 5xFAD (6 m.o.) mice treated with CBM, as evidenced by the reduced number of amyloid depositions (Congo red staining, Figure 3G,H) and A β plaques (Figure 3I,J). However, the average A β plaque size was not changed by CBM (Figure S7E-G). A persistent significant increase of area fraction of MLVs (LYVE-1⁺) in the superior sagittal sinus (Figure 3K,L) and transverse sinus (Figure 3M,N), but not at the confluence of sinus (Figure 3O), can still be observed in 5xFAD (6 m.o.) mice treated with CBM. This indicated that in the 5xFAD mouse, the beneficial effects of CBM on meningeal lymphangiogenesis can last for at least 60 days following CBM treatment.

To further investigate the long-term effects of CBM on meningeal lymphatic drainage function, OVA-A647 was I.C.M injected. No significant difference of the area fraction of OVA-A647 in meninges was detected between the two groups (Figure S7H). The area fraction of

OVA-A647 in dCLNs was significantly increased in 5xFAD (6 m.o.) mice treated with CBM (Figure 3P,Q). Sholl analysis demonstrated that neuroinflammation was still alleviated in the 5xFAD (6 m.o.) mice after CBM treatment, as evidenced by the increased microglial ramification in the thalamus (Figure 3R). Collectively, these results suggested that CBM can exert therapeutic effects on AD progression via promoting meningeal lymphangiogenesis and enhancing meningeal lymphatic drainage function in 5xFAD mice for at least 60 days following the CBM procedure.

3.4 | Ablation of MLVs impaired the therapeutic effects of CBM on AD progression

We next investigated the role of MLVs in the therapeutic effects of CBM. MLVs can be selectively ablated by injecting a photodynamic drug, Visudyne (also known as verteporfin for injection), into the CSF, which upon photoconversion has been shown to preferentially damage the meningeal LECs.⁹ Note that this procedure was reported to have no off-target effects in the coverage of meningeal blood vasculature.⁹ Injections of vehicle followed by photoconversion were treated as control group. Visudyne injection and photoconversion were conducted 7 days before CBM surgery (Figure 4A). Visudyne injection with photoconversion resulted in effective ablation of MLVs in the superior sagittal sinus, transverse sinus, and confluence of sinus (Figure 4B), with the ablation effects lasting for at least 4 weeks (Figure 4C-E). Moreover, the area fraction of OVA-A647 in the meninges of 5xFAD mice was significantly decreased after photodynamic treatment (Figure S8A), and the drainage function of MLVs was also significantly impaired, as evidenced by the reduced area fraction of OVA-A647 in dCLNs of 5xFAD mice in the Visudyne+laser group compared to other groups (Figure 4F,G).

To further investigate the role of MLVs in CBM, Visudyne/vehicle injection and photoconversion were conducted 7 days before the CBM surgery. Behavioral tests were conducted to evaluate memory functions of 5xFAD mice when CBM procedures were completed (Figure 4A). In the open field test, no significant changes were observed for total distance and time in central zone (Figure S8B,C) in 5xFAD mice across the different groups. In the NOR test, the discrimination index (Figure 4H) and preference index (Figure 4I) were significantly improved in Vehicle+Laser+CBM group, whereas such improvement was significantly abolished by the ablation of MLVs. In the Barnes maze test, the escape latency was significantly decreased in the Vehicle+Laser+CBM group during acquisition phase (Figure 4J). During the probe test phase, no significant difference in total travel distance was detected among the groups (Figure S8D), and Vehicle+Laser+CBM group mice spent more time in the target quadrant, whereas such improvement in memory function was significantly impaired by the ablation of MLVs (Figure 4K,L). Histopathological results revealed significantly reduced amyloid depositions (Figure 4M,N) and A β plaques (Figure 4O,P) in the thalamus of Vehicle+Laser+CBM group mice, as evidenced by the reduced number of amyloid depositions and A β plaques but not average A β plaque size

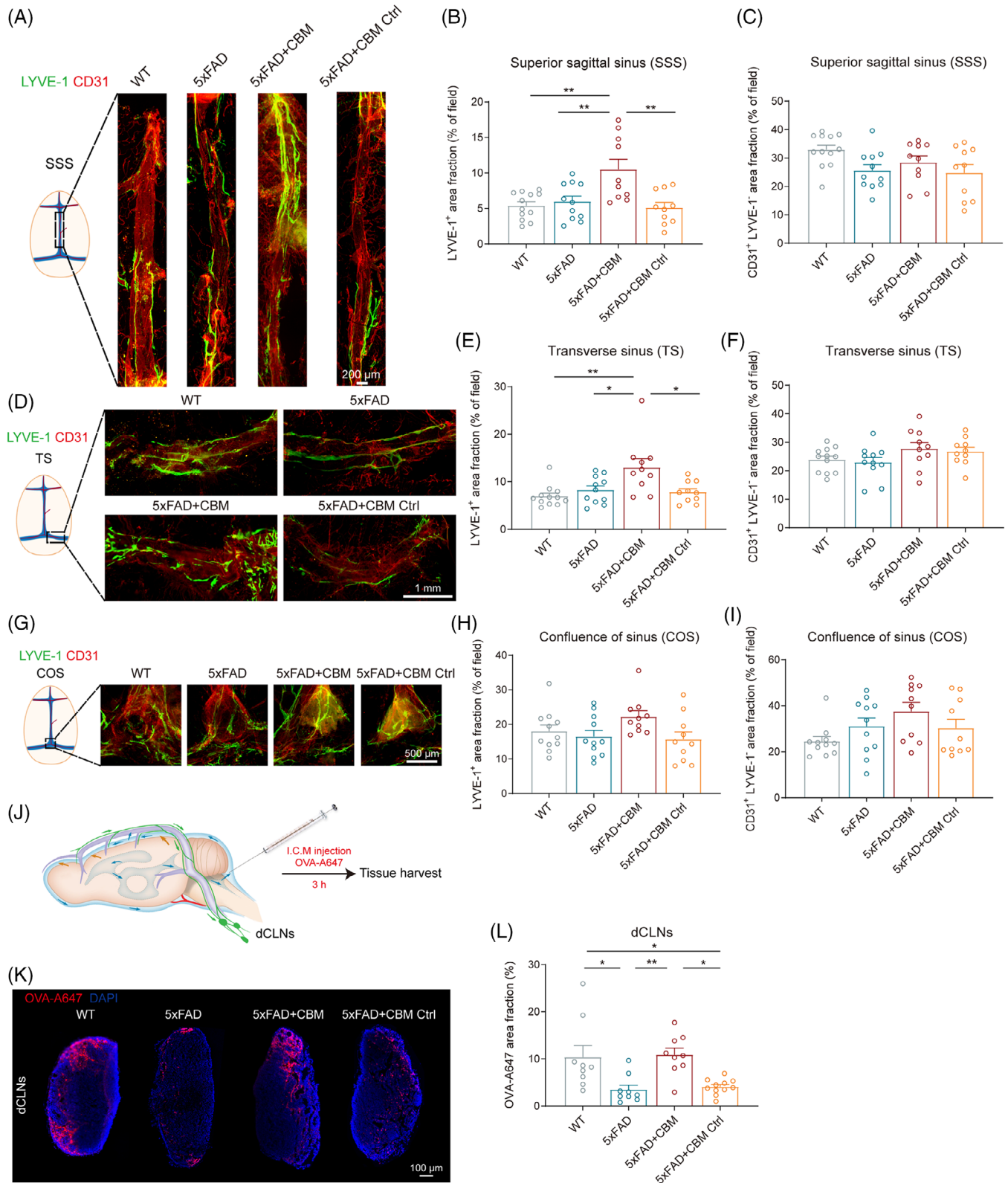


FIGURE 2 CBM promoted meningeal lymphangiogenesis and enhanced meningeal lymphatic drainage function in 5xFAD mice. (A–I) CBM significantly promoted meningeal lymphangiogenesis (LYVE-1⁺) but not angiogenesis (CD31⁺LYVE-1⁻) in the superior sagittal sinus (A–C) and transverse sinus (D–F) of 5xFAD mice, whereas no significant changes were observed in the confluence of sinus (G–I), $n = 10–12$ mice/group. (J) After I.C.M. injection of OVA-A647 (reproduced with permission from *Neuron*. 2016 Sep 7;91(5):957–973³⁶), (K and L) CBM significantly enhanced meningeal lymphatic drainage function in 5xFAD mice, $n = 9–11$ mice/group. Values are means \pm SEM. * $p < 0.05$, ** $p < 0.01$, one-way ANOVA with Bonferroni's post hoc tests among groups were used. ANOVA, analysis of variance; CBM, cranial bone maneuver; dCLNs, deep cervical lymph nodes; I.C.M., intra-cisterna magna; SEM, standard error of the mean.

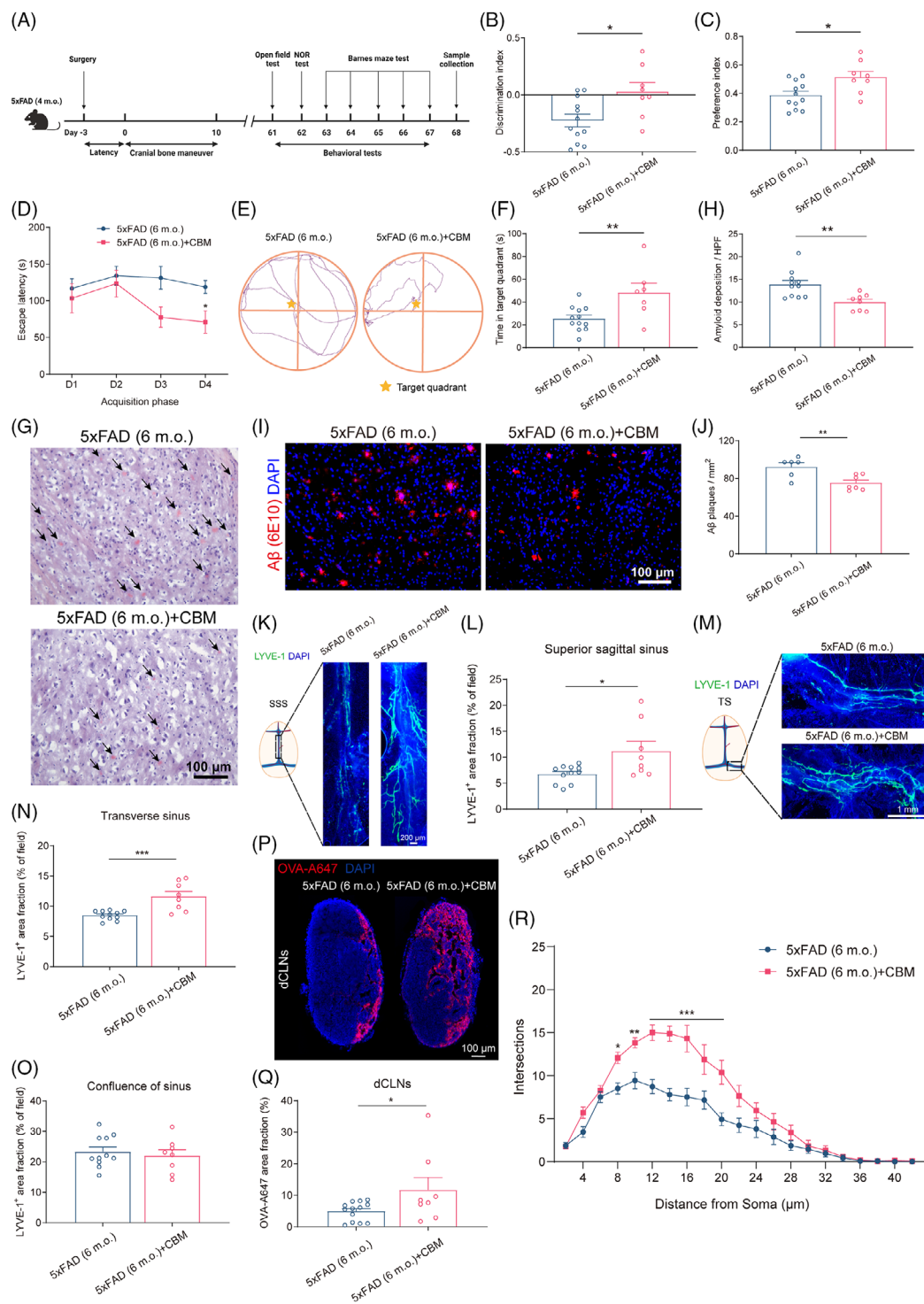


FIGURE 3 The long-term effects of CBM on memory functions, amyloid depositions and A β plaques, and neuroinflammation of 5xFAD mice. **(A)** Experimental schedule for assessing the long-term effects of CBM. For the NOR test, the discrimination index **(B)**, and preference index **(C)** were significantly increased in 5xFAD mice treated with CBM. **(D–F)** In the Barnes maze test, CBM significantly improved the spatial memory functions of 5xFAD mice, with the escape latency significantly decreased and the time in the target quadrant significantly increased, $n = 8–12$ mice/group. CBM significantly reduced amyloid depositions (as black arrows indicated, **G** and **H**) and A β plaques (**I** and **J**) in the thalamus of 5xFAD mice, $n = 6–10$ mice/group. CBM significantly promoted meningeal lymphangiogenesis in the superior sagittal sinus (LYVE-1 $^{+}$, **K**, and **L**) and the transverse sinus (**M** and **N**) but not in the confluence of sinus (**O**) of 5xFAD mice, $n = 8–11$ mice/group. **(P** and **Q**) After I.C.M injection of OVA-A647, CBM significantly enhanced meningeal lymphatic drainage function in 5xFAD mice; $n = 8–13$ mice/group. **(R)** Sholl analysis revealed that neuroinflammation of 5xFAD mice was significantly alleviated after the treatment of CBM; $n = 5$ mice/group. Values are means \pm SEM. * $p < 0.05$, ** $p < 0.01$, and *** $p < 0.001$, Student's t test, and two-way ANOVA with Bonferroni's post hoc tests among groups were used. ANOVA, analysis of variance; CBM, cranial bone maneuver; dCLNs, deep cervical lymph nodes; HPF, high-power field; I.C.M, intra-cisterna magna; NOR, novel object recognition; SEM, standard error of the mean.

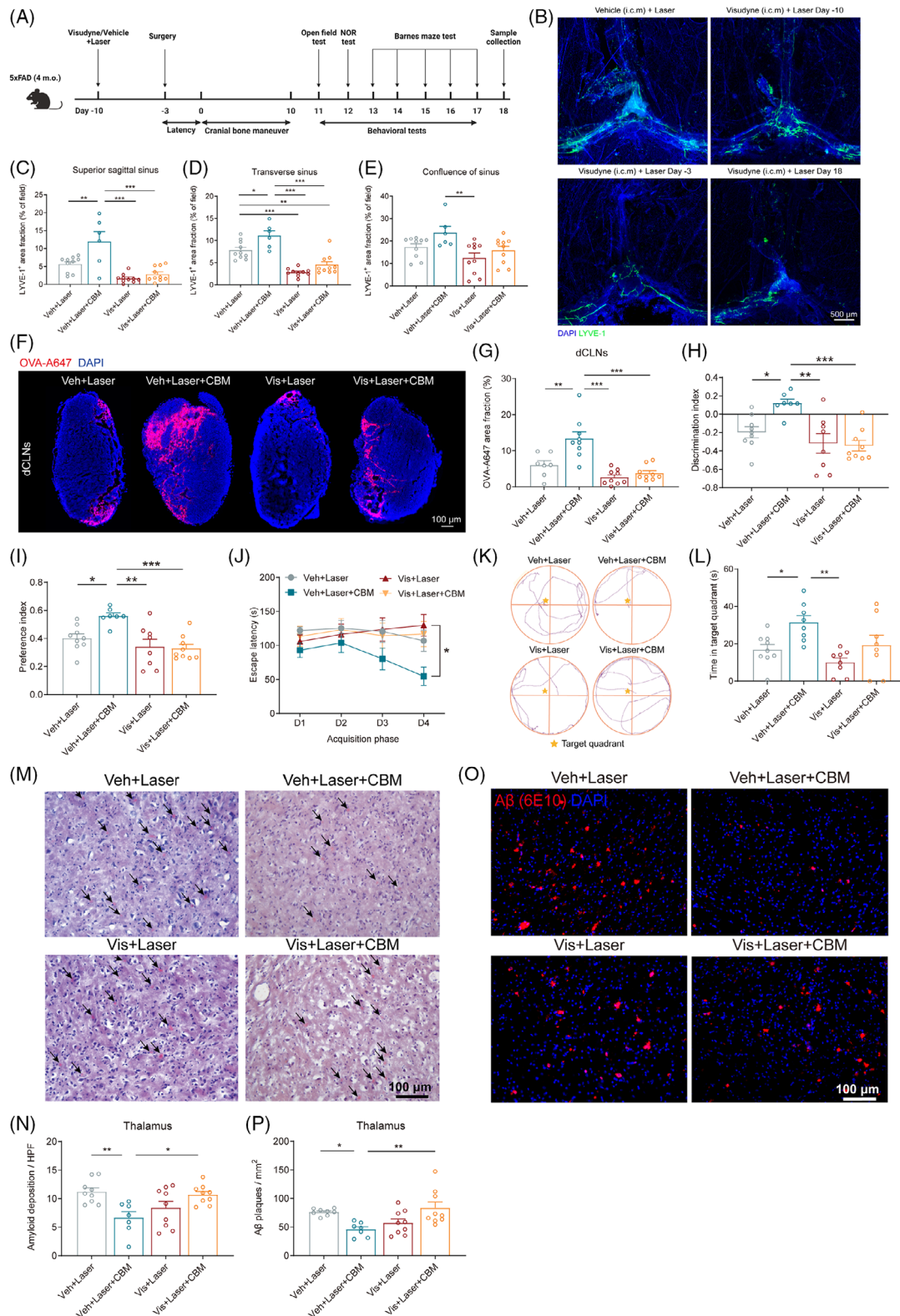


FIGURE 4 Ablation of MLVs impaired the therapeutic effects of CBM. (A) Experimental schedule for the ablation of MLVs, CBM treatment and behavioral tests. (B–E) Using “Visudyne+Laser” method, MLVs (LYVE-1+, B) in superior sagittal sinus (C), transverse sinus (D), and confluence of sinus (E) were successfully ablated, which can last for more than 4 weeks; $n = 6–10$ mice/group. (F and G) The meningeal lymphatic drainage function was also significantly impaired after the ablation of MLVs. For the NOR test (H and I) and Barnes maze test (J–L), ablation of MLVs significantly impaired CBM-induced memory function improvement and the decrease of amyloid depositions (as black arrows indicated, M and N) and A β plaques (O and P) in the thalamus of 5xFAD mice; $n = 7–9$ mice/group. Values are means \pm SEM. * $p < 0.05$, ** $p < 0.01$, and *** $p < 0.001$, one-way or two-way ANOVA with Bonferroni’s post hoc tests among groups. ANOVA, analysis of variance; CBM, cranial bone maneuver; dCLNs: deep cervical lymph nodes; HPF, high-power field; MLVs, meningeal lymphatic vessels; NOR, novel object recognition; SEM, standard error of the mean.

(Figure S8E–G). However, such amelioration effects were significantly impaired by ablation of MLVs. In summary, MLVs are indispensable elements for CBM treatment therapeutic effects in the 5xFAD mouse.

3.5 | Inflammatory processes in the skull and meninges after CBM treatment

After 10 days of CBM treatment, skull and meninges were harvested to evaluate the mRNA and protein levels of inflammatory and lymphangiogenic factors (Figure 5A). CBM significantly increased the mRNA levels of *Il-1 β* , *Il-6*, and *Vegf-c* (Figure 5B–D), but not *Tgf- β* and *Tnf- α* in the skull (Figure S9A,B). The protein levels of IL-1 β and IL-6 were significantly increased in the skull treated with CBM (Figure 5E–G), but not IL-10 and TGF- β (Figure S9C,D). Intriguingly, prominent osteogenic structure can be observed near the surgical site in the skull of CBM group, whereas fibrosis structure was observed in the skull of CBM control group (Figure 5F). VEGF-C and VEGF-D are both known as lymphangiogenic factors³⁸; the protein levels of VEGF-D, but not VEGF-C were significantly increased in the skull treated with CBM (Figure 5H,I). CBM significantly increased the protein levels of VEGF-C and TGF- β (Figure 5J,K), but not IL-1 β , IL-6, IL-10, and VEGF-D in the meninges (Figure S9E–H).

Myeloid cells consist of the majority of innate immune cells in the skull marrow.³⁹ Recent studies suggested that tissue-resident macrophages can detect the mechanical properties of the extracellular matrix to regulate a specific tissue repair program.⁴⁰ By moving the bone flap in vertical directions (upward and downward displacement) along the days, mechanical stimulation was assumed to be applied to the skull marrow during CBM procedures. The current study further explored the effects of mechanical stimulation on macrophages. Single direction of cell stretch was applied to RAW264.7 cells with 10% deformation within 24 h (Figure S10A). The mRNA levels of *Il-6*, *Tgf- β* , and *Vegf-c* were significantly increased after cell stretching, but not *Il-1 β* and *Tnf- α* (Figure S10B–F). Moreover, bidirectional cell stretch was applied to RAW264.7 cells with 10% deformation within 48 h (Figure S10G). The mRNA levels of *Il-6* and *Tgf- β* were persistently increased after cell stretching, but not *Il-1 β* , *Tnf- α* , and *Vegf-c* (Figure S10H–L).

3.6 | Transcriptional profiles of the meninges after CBM treatment

As CBM significantly promoted lymphangiogenesis and persistently enhanced the meningeal lymphatic drainage function, we harvested meninges to conduct RNA-seq analysis and investigated DEGs following CBM treatment. Compared with 5xFAD mice, transcriptomic analyses revealed that 4582 genes (1984 upregulated and 2598 downregulated) were differentially expressed in the meninges on day 10 of CBM procedures (Figure 5L). Intriguingly, the majority genes responsible for lymphangiogenesis⁴¹ were found to be upregulated in the meninges after CBM treatment (Figure 5M). Among the upregu-

lated DEGs, KEGG pathway enrichment analysis revealed that 122 upregulated DEGs were enriched in multiple inflammation regulations, including cytokine–cytokine receptor interaction, chemokine signaling pathway, B cell receptor signaling pathway and TNF signaling pathway (Figure 5N). GO enrichment analysis revealed that 228 upregulated DEGs were enriched in multiple immune-related processes, including inflammatory responses, immune system process, immune response, innate immune response, positive regulation of IL-6 production, cytokine-mediated signaling pathway, and Fc-gamma receptor signaling pathway (Figure S11A). These results suggest a key role in immune responses in the process of CBM-induced lymphangiogenesis. Moreover, tissue enrichment analysis indicated that the upregulated DEGs are predominantly associated with macrophages and mast cells in the meninges following CBM treatment (Figure 5O). Further investigations revealed that the density of macrophages but not mast cells in meninges was significantly increased near the osteotomy and CBM sites, along with a significant elevated level of VEGF-C in the meninges (Figure 5P and Figure S11B). Furthermore, 19 upregulated DEGs were related to macrophage functions (Figure S11C). Of interest, we have also identified substantial interactions between these genes and the upregulated genes involved in the lymphangiogenesis pathway (Figure S11D). These findings indicated that the CBM procedure likely induces cascades of inflammatory responses and lymphangiogenesis processes in the meninges of 5xFAD mice for exerting its therapeutic effects.

3.7 | The effects of IL-6 on LECs

Previous studies have suggested that injury-induced IL-6 drives lymphangiogenesis in bone.⁴² Human dermal LECs (Figure S12) and human recombinant IL-6 protein were used to investigate the effects of IL-6 on LECs in vitro. This study found that IL-6 can significantly promote the proliferation of human dermal LECs with the concentration of 20 ng/mL (Figure 6A,B). The mRNA levels of *Il-1 β* , *Il-6*, and *CCL2* in LECs were significantly increased after 48 h of treatment of IL-6, but not *TGF- β* , *CCL5*, *CXCL1*, and *CX3CL1* (Figure 6C–F and Figure S13A–C). Moreover, IL-6 significantly enhanced tube formation of LECs with the increase of the total length and number of branches, whereas Tocilizumab (IL-6R antibody) blocked such enhancement (Figure 6G–I). IL-6 can also promote the migration of LECs with significant increase of wound closure percentage after 12 and 24 h, whereas Tocilizumab blocked such enhancement (Figure 6J–L). Collectively, IL-6 was found to promote the proliferation, migration, and tube formation of LECs.

3.8 | Pharmacological inhibition of the VEGF-C/VEGFR3 pathway impaired the therapeutic effects of CBM on AD progression

Meningeal lymphangiogenesis was inhibited by I.C.M infusion of MAZ51 (inhibitor of VEGFR3 tyrosine kinase) for 4 weeks using an osmotic pump (Figure 7A,B). Infusion of vehicle solution was applied to

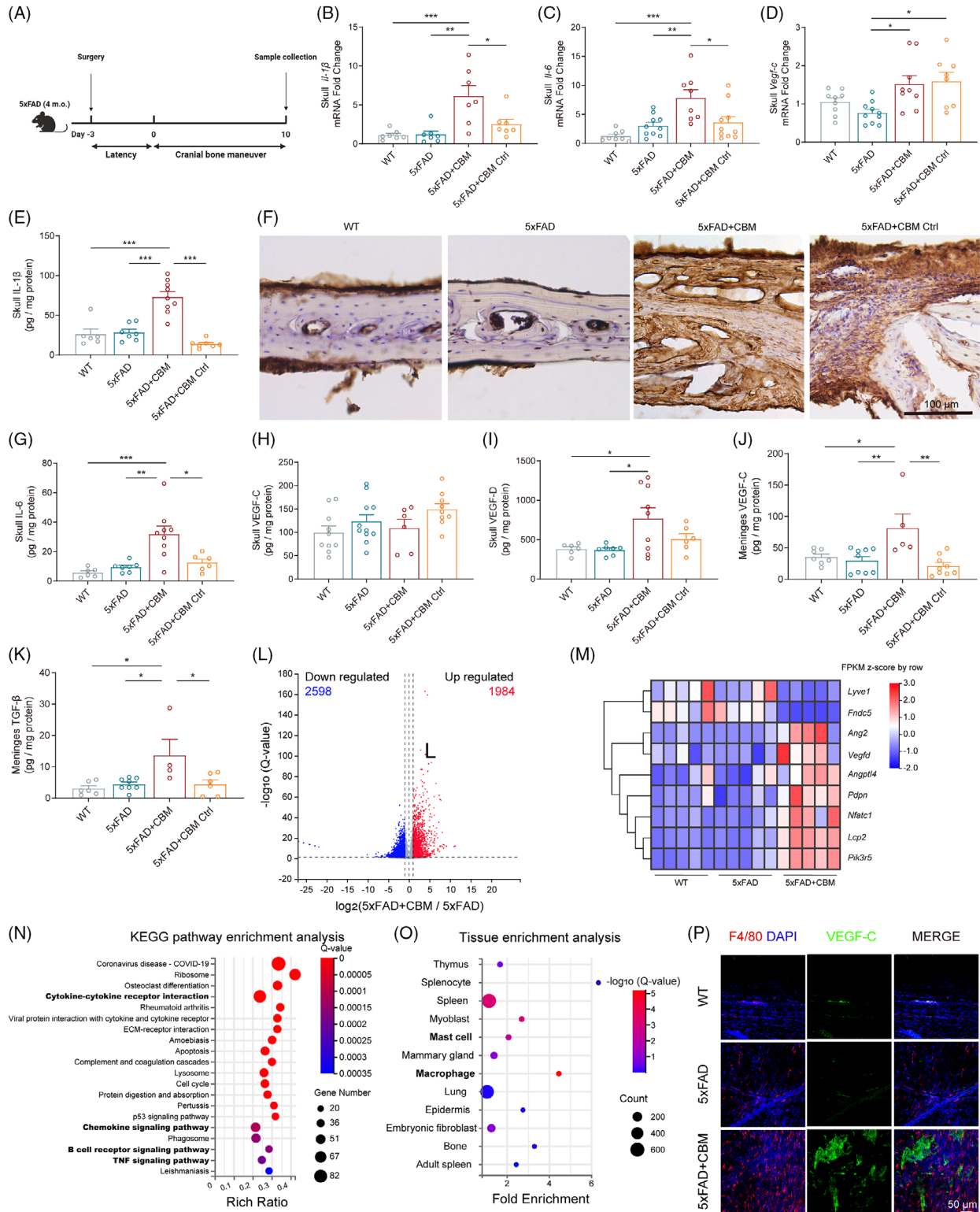


FIGURE 5 Inflammatory and lymphangiogenic processes in skull and meninges after CBM treatment. (A) Experimental schedule for sample collection after CBM treatment. The changes of mRNA levels of *Il-1β* (B), *Il-6* (C), and *Vegf-c* (D) in skull after CBM treatment. The changes of protein levels of *IL-1β* (E), *IL-6* (F representative immunohistochemical staining of *IL-6*, and G), *VEGF-C* (H), and *VEGF-D* (I) in skull after CBM treatment. The changes of protein levels of *VEGF-C* (J) and *TGF-β* (K) in meninges after CBM treatment. RNA-seq analysis reveals the transcriptional changes of the meninges after CBM treatment. (L) Volcano map of DEGs in meninges of 5xFAD mice at day 10 of CBM procedures. (M) Heatmap of DEGs enriched in the lymphangiogenesis pathway gene set. (N) KEGG pathway enrichment analyses of upregulated DEGs. (O) Tissue enrichment analysis indicated that the upregulated DEGs were enriched in macrophages and mast cells in meninges after CBM treatment. (P) Representative images of the distribution pattern of macrophages (F4/80⁺) and VEGF-C in meninges of 5xFAD mice proximal to the surgical site. **p* < 0.05, ***p* < 0.01, and ****p* < 0.001, one-way ANOVA with Bonferroni's post hoc tests among groups. ANOVA, analysis of variance; CBM, cranial bone maneuver; DEGs, differentially expressed genes; mRNA, messenger RNA.

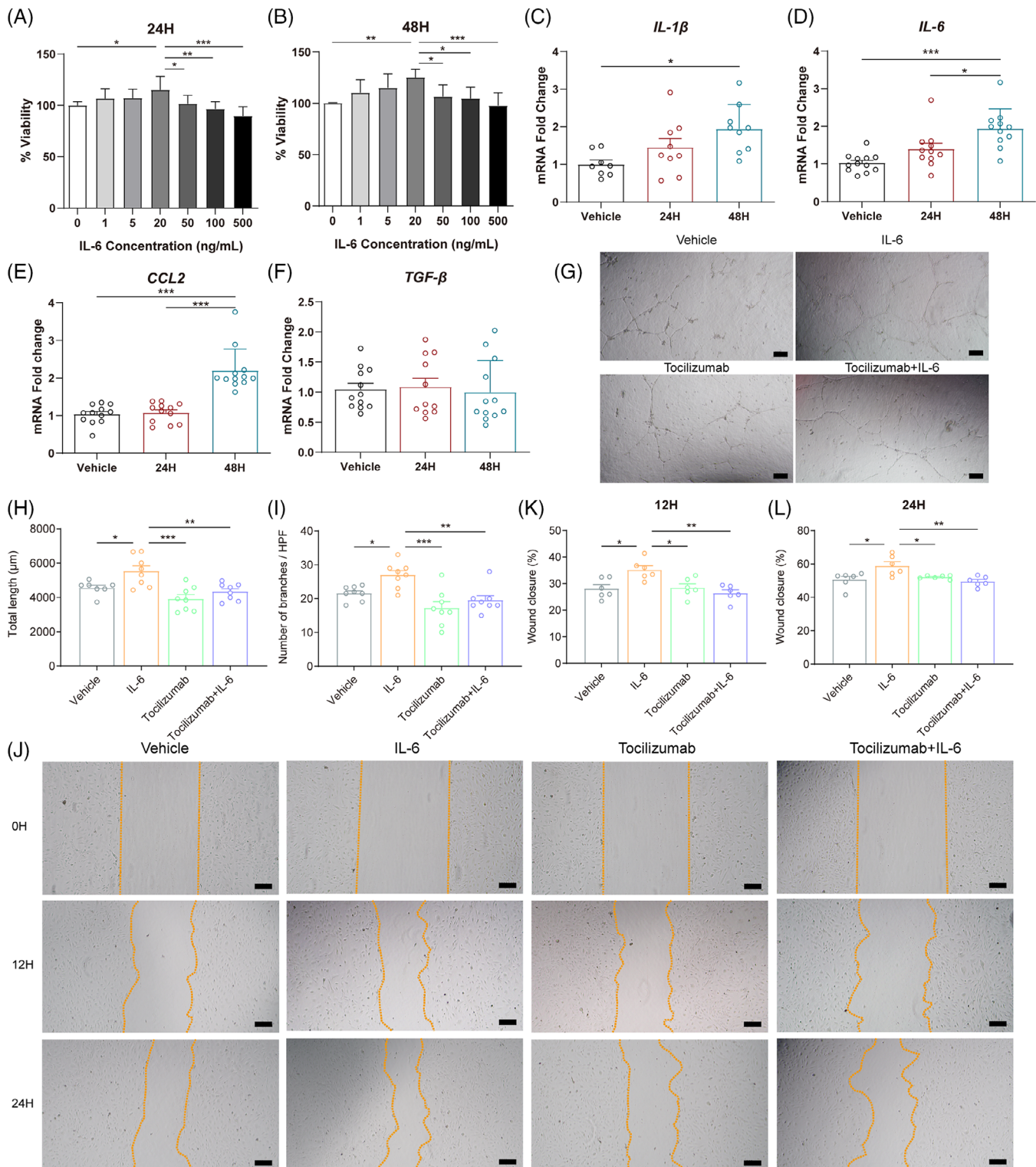


FIGURE 6 The effects of IL-6 on LECs. (A and B) Cell viability of human dermal LECs exposed to IL-6 for 24 and 48 h was measured using the CCK-8 assay. The changes of mRNA levels of *IL-1 β* (C), *IL-6* (D), *CCL2* (E), and *TGF- β* (F) in human dermal LECs after IL-6 treatment for 24 and 48 h. For tube-formation assay (G), IL-6 significantly increased the total length (H) and number of branches (I) of LECs, whereas Tocilizumab blocked such enhancement effect. For cell scratch assay (J), IL-6 promotes the migration of LECs with significant increase of wound closure percentage after 12 (K) and 24 h (L), whereas Tocilizumab blocked such enhancement. * $p < 0.05$, ** $p < 0.01$, and *** $p < 0.001$, one-way ANOVA with Bonferroni's post hoc tests among groups. ANOVA, analysis of variance; CBM, cranial bone maneuver; LECs, lymphatic endothelial cells.

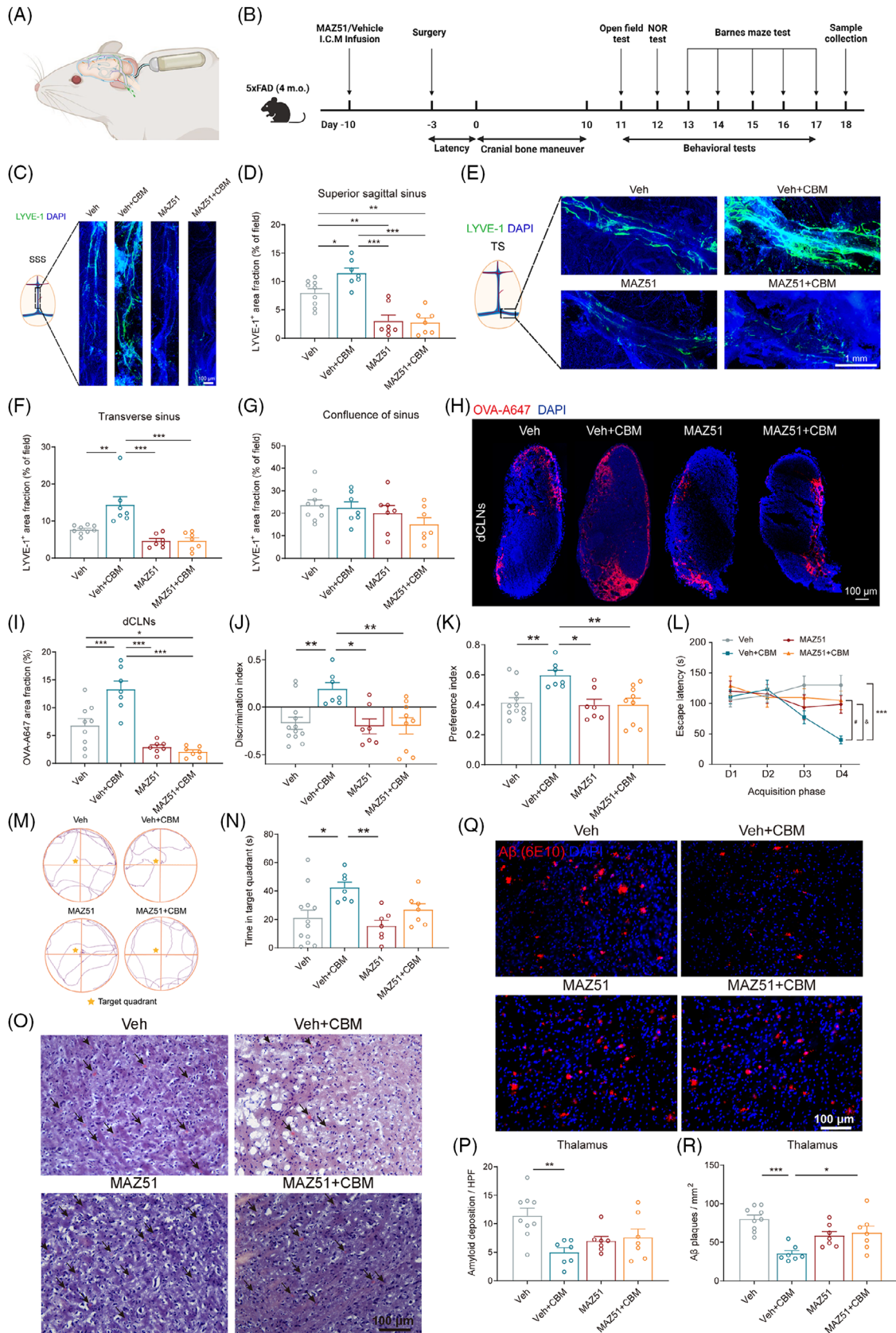


FIGURE 7 Pharmacological inhibition of VEGF-C/VEGFR3 pathway impaired the therapeutic effects of CBM on AD. (A) Schematic graph of osmotic pump I.C.M infusion. (B) Experimental schedule for pharmacological inhibition of VEGF-C/VEGFR3 pathway and behavioral tests. After I.C.M infusion of MAZ51, MLVs in the superior sagittal sinus (C and D) and transverse sinus (E and F), but not in the confluence of sinus (G), were significantly eliminated. The meningeal lymphatic drainage function was significantly impaired after the inhibition of VEGF-C/VEGFR3 pathway (H

the control group. The MLVs in the superior sagittal sinus (Figure 7C,D) and transverse sinus (Figure 7E,F), but not at the confluence of sinus (Figure 7G), were eliminated after 4 weeks of I.C.M infusion of MAZ51. No difference in area fraction of OVA-A647 in the meninges was seen among the groups following MAZ51 infusion (Figure S14A), and the drainage function of MLVs was significantly impaired, as evidenced by the reduced area fraction of OVA-A647 in dCLNs of 5xFAD mice in the MAZ51 groups with or without CBM treatment compared to the vehicle groups (Figure 7H,I).

To further investigate the role of VEGF-C/VEGFR3 pathway in CBM, I.C.M infusions with MAZ51/vehicle were conducted 7 days before CBM surgery. Behavioral tests were conducted to evaluate the locomotion activities and memory functions of 5xFAD mice when CBM treatment was completed (Figure 7B). In the open field test, no significant changes were observed for total travel distance and time in central zone in 5xFAD mice among groups (Figure S14B,C). In the NOR test, the discrimination index (Figure 7J) and preference index (Figure 7K) were significantly improved in the Vehicle+CBM group, whereas such improvement was significantly impaired by blocking the VEGF-C/VEGFR3 signaling pathway. In the Barnes maze test, the escape latency was significantly decreased in the Vehicle+CBM group during acquisition phase (Figure 7L). During the probe test phase, no significant difference of total travel distance was detected among groups (Figure S14D), and Vehicle+CBM group mice spent more time in the target quadrant (Figure 7 M,N), whereas such memory function improvement was significantly impaired by blocking the VEGF-C/VEGFR3 pathway. Histopathological results revealed a significant dampening in amyloid depositions (Figure 7O,P, Figure S14E) and A β plaques (Figure 7Q,R and Figure S14F) in the cortex and thalamus of Vehicle+CBM group mice, as evidenced by the reduced number of amyloid depositions and A β plaques rather than average A β plaque size (Figure S14G-I). However, such ameliorating effects were significantly impaired by the blockage of VEGF-C/VEGFR3 pathway. In summary, these results indicated that CBM may promote meningeal lymphangiogenesis and enhance meningeal lymphatic drainage function via the VEGF-C/VEGFR3 pathway.

4 | DISCUSSION

The current study reported that CBM treatment significantly promoted meningeal lymphangiogenesis and enhanced meningeal lymphatic drainage function in 5xFAD mice, resulting in improvement of memory functions, reduction of amyloidosis in brain, and alleviation of neuroinflammation. It is important to note that the therapeutic effects

of CBM treatment in 5xFAD mice lasted for at least 2 months—a considerably long duration for mice. Specific photoablation of the dorsal MLVs significantly abolished the drainage function of MLVs in 5xFAD mice, and subsequently counteracted the therapeutic effects of CBM treatment. Using RNA-seq analysis, we found that CBM treatment induced cascades of inflammatory responses and lymphangiogenic processes in the meninges of 5xFAD mice, which are critical for the therapeutic effects. Pharmacological inhibition of VEGF-C/VEGFR3 pathway predominantly eliminated MLVs, abolished the drainage function of MLVs in 5xFAD mice, and diminished the therapeutic effects of CBM on AD progression.

The DH technique has been applied beyond bone repair, demonstrating its potential in tissue regeneration. Studies have shown that DH procedure increased the muscle fibers and volume in patients undergoing bone lengthening.^{43,44} DH stimulates angiogenesis in the newly formed bone tissue, with new blood vessels being most abundant in the distraction phase and maintaining for the entire treatment duration.⁴⁵ Gradual tension-stress stimulation during DH treatment promotes regeneration of various tissues. Similarly, CBM treatment significantly promotes meningeal lymphangiogenesis and enhances meningeal lymphatic drainage function. A similar phenomenon was observed in other cranial bone surgical procedures in mice. A previous study found that chronically implanted electroencephalography electrodes induced significant lymphangiogenesis near the osteotomy site, along with widespread reactive gliosis and increased CSF influx.⁴⁶ Delivery of adeno-associated virus-VEGF-C has been reported to induce lymphangiogenesis in the meninges and enhanced meningeal lymphatic drainage to the dCLNs.^{47,48} However, adeno-associated virus mediated therapy may cause cerebellar toxicity in nonhuman primate,⁴⁹ which remains controversial. In contrast, the CBM surgery reported here is a safe, practical, and reproducible method for promoting lymphangiogenesis and enhancing meningeal lymphatic drainage function.

Growing evidence suggests that an imbalance of production and clearance of A β may lead to its accumulation and aggregation in the brain.⁵⁰ Recent work showed that the meningeal lymphatic system and A β clearance are closely linked. A β accumulation may lead to lymphatic dysfunction, which further hinders A β clearance.^{9,15,51} Another study also found that boosting meningeal lymphatics with immunotherapies could enhance A β clearance and reduce the detrimental microglial inflammatory response in AD animals.³⁵ The age-associated impairment of MLVs may contribute to cognitive decline.¹⁵ In fact, aged mice showed reduced brain perfusion compared to their young counterparts and was accompanied by a reduction in the diameter and coverage of MLVs, as well as decreased drainage of CSF

and I). For the NOR test (J and K) and Barnes maze test (L-N), inhibition of the VEGF-C/VEGFR3 pathway significantly impaired CBM-induced memory function improvement, compared to the vehicle groups; $n = 7-12$ mice/group. Representative images of Congo red staining (as black arrows indicated, O) and quantification results of amyloid depositions in thalamus (P) of 5xFAD mice. Representative images of immunofluorescence staining (Q) and quantification results of A β plaques in thalamus (R) of 5xFAD mice. $n = 7-9$ mice/group. Values are means \pm SEM. * $p < 0.05$, ** $p < 0.01$, and *** $p < 0.001$, one-way or two-way ANOVA with Bonferroni's post hoc tests among groups were used. ANOVA, analysis of variance; CBM, cranial bone maneuver; dCLNs, deep cervical lymph nodes; HPF, high-power field; I.C.M, intra-cisterna magna; MLVs, meningeal lymphatic vessels; NOR, novel object recognition; SEM, standard error of the mean.

into dCLNs.¹⁵ Our results revealed that CBM enhanced the clearance of A β plaques through the meningeal lymphatic pathway, which could last long even after ceasing the bone maneuver. Inflammation can cause the growth of new initial lymphatics, a process known as lymphangiogenesis, in both the draining lymph node and inflamed tissue.⁵² Previous studies have suggested that both IL-6 and VEGF-C are indispensable for lymphangiogenesis.⁴² The channels between skull marrow and meninges may play an important role in cellular and molecular communications. IL-6 increases VEGF-C induction and lymphangiogenesis, which may involve the Src-FAK-STAT3 cascade in LECs.⁵³ In addition, this study found that IL-6 increases CCL2 induction in LECs, which may contribute to macrophages chemotaxis to meninges.⁵⁴ VEGF-C released by macrophages under stimulation of various inflammatory cytokines is a key mediator for inflammation-induced lymphangiogenesis.⁵⁵ Tension stress can promote lymphangiogenesis through the VEGF-C-independent VEGFR3 signaling pathway.⁵⁶ In the meantime, macrophages also promote IL-6, TGF- β , and VEGF-C production under mechanical stimulation, which may further support meningeal lymphangiogenesis. Therefore, both the local inflammation and mechanical stimulation incurred during CBM treatment may initiate and maintain the long-term enhancement effects on meningeal lymphangiogenesis and the meningeal lymphatic drainage function.

The therapeutic mechanisms highlighted in our study are also clinically relevant. Previous study showed that ablation of MLVs in 5xFAD mice compromised the therapeutic effects of anti-A β passive immunotherapy with increased A β deposition, microgliosis and worsened neurovascular dysfunction and behavioral deficits.³⁵ Intriguingly, the gene expression patterns of microglia from 5xFAD mice with dysfunctional MLVs substantially resembled the transcriptional profiles of microglia in patients with AD, suggesting that the impaired drainage function of MLVs will worsen the microglial inflammatory response in these patients.³⁵ In the current study, ablation of MLVs diminished the therapeutic effects of CBM on AD progression, highlighting the crucial role of MLVs in modulating neurological disorders. Recent studies confirmed the critical role of the MLVs in modulating immune responses and inflammation in the CNS of various disease models.^{57,58} Under physiological conditions, drainage of macromolecules and protein aggregates from the brain through the meningeal lymphatics is essential for maintaining CNS homeostasis. MLVs have the potential to remove neurotropic viruses from the CNS and transport them to dCLNs. When the lymphatic vessels were surgically ligated or the dorsal MLVs were ablated in the virus-infected mice, increased neurological damage and mortality were observed.⁵⁹ Moreover, the impairment of meningeal lymphatics in mice is a contributing factor to their susceptibility to stress, and restoring the meningeal lymphatics function reduced depression-like behavior in mice.⁴⁷

Lymphangiogenesis refers to the process of sprouting and proliferation of LECs and formation of lymphatic vessels. Myeloid cells appear to play an important role in meningeal tissue remodeling, which can direct ectopic lymphangiogenesis in the spinal cord meninges after injury.⁶⁰ In agreement with these reports, our results found a significant increase in macrophage density around the CBM sites, which

may be responsible for promoting lymphangiogenesis and strengthening drainage function of MLVs. In a recent study, four different subsets of meningeal macrophages were identified based on the expression of markers CD38, LYVE-1, MHC II, and CCR2. These meningeal macrophages play diverse roles in tissue homeostasis, debris clearance, and infection protection.⁶¹ During the development of LYVE-1⁺/Prox-1⁺ lymphatic vessels, an abundant subpopulation of LYVE-1⁺/PROX-1⁻/CD206⁺/F4/80⁺ macrophage-like cells was observed, which gradually disappeared during further lymphatic vessels development possibly due to Lyve-1 downregulation.⁶² When the VEGF-C/VEGFR3 signaling pathway was blocked, the growth and survival of LECs were inhibited, and the same subpopulation cells appeared again.⁶³ Further investigations are still needed to explore the roles of meningeal macrophages in lymphangiogenesis during CBM treatment.

Our results underscored that the therapeutic effects of CBM are dependent on VEGF-C/VEGFR3 signaling pathway. The VEGF-C/VEGFR3 pathway is a promising therapeutic target for CNS disorders. Intracerebroventricular injection of adeno-associated virus-VEGF-C stimulated meningeal lymphangiogenesis without compromising the function of meningeal blood vessels or the blood-brain barrier. Augmentation of MLVs and their drainage capacity using lymphangiogenic growth factor provides therapeutic benefits for AD, stroke, traumatic brain injury, neurotropic viral infection, and even hepatic encephalopathy in cirrhosis.^{10,12,15,59,64} In this regard, CBM appears to be a simple and effective method for stimulating MLVs expansion and improving the outflow of fluid, cells, and macromolecules in the current study. Further clinical studies are warranted to apply CBM as a new treatment for neuropathological disorders.

There are some limitations of the present study. First, previous studies indicated that basal MLVs are more active in CSF drainage than the dorsal lymphatics,³⁴ and that CSF primarily flows through the basal MLVs rather than the dorsal region.⁶⁵ Both the dorsal and basal dural lymphatic vessels contribute to the drainage of CSF; however, the current study solely explored the lymphangiogenic effects of CBM on dorsal MLVs owing to limited technical capabilities. Second, sporadic AD is a neurodegenerative disease that progresses slowly, characterized by gradual decline in memory and cognitive abilities. However, this study investigated only the therapeutic effects of CBM in transgenic AD mice at early pathological phase, which may not fully demonstrate the entire therapeutic effects and potential impacts of CBM. In addition, this study only used Sholl analysis to evaluate neuroinflammation. Measurements of proinflammatory cytokines and canonical markers of microglial activation are required in our future study. Third, MAZ51 inhibits a variety of kinases other than VEGFR3. Its side effects should not be neglected. Alternative approaches using anti-VEGFR-3 blocking antibodies, soluble VEGFR-3 (VEGF-C trap), or a mouse model with lymphatic *Vegfr3*-deletion should be used in future investigations. Finally, innate immune cells are present within the skull marrow and meninges in both normal and inflammatory circumstances. However, there is still limited understanding of how these immune cells interact with the LECs for regulating lymphangiogenesis.

In summary, the current study investigated the therapeutic effects of CBM on AD progression using 5xFAD mice. CBM procedures

improved memory functions, reduced amyloidosis, alleviated neuroinflammation, and promoted meningeal lymphangiogenesis and lymphatic drainage function through the VEGF-C/VEGFR3 pathway. The beneficial effects of CBM lasted for a relatively long period after the CBM procedure. RNA-seq analysis revealed that CBM can induce cascades of inflammatory responses and lymphangiogenesis processes in the meninges of 5x*FAD* mice to exert therapeutic effects. CBM significantly increased the protein levels of IL-1 β and IL-6 in the skull and VEGF-C in the meninges. IL-6 was proven to promote the proliferation, migration, and tube formation of LECs. Photoablation of MLVs and blockage of the VEGF-C/VEGFR3 pathway diminished the therapeutic effects of CBM on AD progression. These findings suggest that CBM might be a novel promising approach for AD management by augmenting the meningeal lymphatic drainage function. Further clinical investigations are highly warranted.

ACKNOWLEDGMENTS

The authors thank Prof. Kai Liu (The Hong Kong University of Science and Technology) for providing insightful suggestions. We also thank Dr. Eugene Ponomarev, Dr. Hao Lyu, Dr. Mingde Cao, and Ms. Mengran Xiong (The Chinese University of Hong Kong) for their help with this study. This work was supported by grants from the National Natural Science Foundation of China (82172430, 82272505, 82472454, 81874000, and 82122001), University Grants Committee, Research Grants Council of the Hong Kong Special Administrative Region, China (14108720, 14121721, 14202920, 14100122, 14119124, 14113723, N_CUHK472/22, C7030-18G, C6027-19GF, C7074-21GF, T13-402/17-N, AoE/M-402/20, and AoE/M-604/16), Heath Medical Research Fund (HMRF) of Food and Health Bureau Hong Kong (17180831, 08190416, and 09203436), Hong Kong Innovation Technology Commission Funds (PRP/050/19FX), and Natural Science Foundation of Guangdong Province (2023A1515011040). This study also received support from the research funds from Health@InnoHK program launched by Innovation Technology Commission of the Hong Kong SAR, PR China.

CONFLICT OF INTEREST STATEMENT

The authors declare no conflicts of interest. Author disclosures are available in the [Supporting Information](#).

CONSENT STATEMENT

The authors have confirmed that consent was not necessary.

ORCID

Gang Li  <https://orcid.org/0000-0002-3981-2239>

REFERENCES

- Ilizarov GA. The tension-stress effect on the genesis and growth of tissues: part II. The influence of the rate and frequency of distraction. *Clin Orthop Relat Res*. 1989(239):263-285.
- Ilizarov GA. The tension-stress effect on the genesis and growth of tissues. Part I. The influence of stability of fixation and soft-tissue preservation. *Clin Orthop Relat Res*. 1989(238):249-281.
- Kong L-C, Li HA, Kang Q-L, Li G. An update to the advances in understanding distraction histogenesis: from biological mechanisms to novel clinical applications. *J Orthop Transl*. 2020;25:3-10. doi:10.1016/j.jot.2020.09.003
- Bai S, Lu X, Pan Q, et al. Cranial bone transport promotes angiogenesis, neurogenesis, and modulates meningeal lymphatic function in middle cerebral artery occlusion rats. *Stroke*. 2022;53(4):1373-1385. doi:10.1161/STROKEAHA.121.037912
- Bouletreau PJ, Warren SM, Paccione MF, Spector JA, McCarthy JG, Longaker MT. Transport distraction osteogenesis: a new method to heal adult calvarial defects. *Plast Reconstr Surg*. 2002;109(3):1074-1084. doi:10.1097/00006534-200203000-00046
- Djachkov AN, Khudiaevev AT, Prudnikova OG. Application of External Fixation in Skull Surgery. In: Solomin L, ed. *The Basic Principles of External Skeletal Fixation Using the Ilizarov and Other Devices*. Springer Milan; 2012:1425-1436.
- Castellani G, Croese T, Peralta Ramos JM, Schwartz M. Transforming the understanding of brain immunity. *Science*. 2023;380(6640):eabo7649. doi:10.1126/science.abo7649
- Kolabas ZI, Kuemmerle LB, Perneczky R, et al. Distinct molecular profiles of skull bone marrow in health and neurological disorders. *Cell*. 2023;186(17):3706-3725 e29. doi:10.1016/j.cell.2023.07.009
- Louveau A, Smirnov I, Keyes TJ, et al. Structural and functional features of central nervous system lymphatic vessels. *Nature*. 2015;523(7560):337-341. doi:10.1038/nature14432
- Bolte AC, Dutta AB, Hurt ME, et al. Meningeal lymphatic dysfunction exacerbates traumatic brain injury pathogenesis. *Nat Commun*. 2020;11(1):4524. doi:10.1038/s41467-020-18113-4
- Chen J, Wang L, Xu H, et al. Meningeal lymphatics clear erythrocytes that arise from subarachnoid hemorrhage. *Nat Commun*. 2020;11(1):3159. doi:10.1038/s41467-020-16851-z
- Hsu SJ, Zhang C, Jeong J, et al. Enhanced meningeal lymphatic drainage ameliorates neuroinflammation and hepatic encephalopathy in cirrhotic rats. *Gastroenterology*. 2021;160(4):1315-1329 e13. doi:10.1053/j.gastro.2020.11.036
- Zhou C, Ma L, Xu H, Huo Y, Luo J. Meningeal lymphatics regulate radiotherapy efficacy through modulating anti-tumor immunity. *Cell Res*. 2022;32(6):543-554. doi:10.1038/s41422-022-00639-5
- Zou W, Pu T, Feng W, et al. Blocking meningeal lymphatic drainage aggravates Parkinson's disease-like pathology in mice overexpressing mutated alpha-synuclein. *Transl Neurodegener*. 2019;8:7. doi:10.1186/s40035-019-0147-y
- Da Mesquita S, Louveau A, Vaccari A, et al. Functional aspects of meningeal lymphatics in ageing and Alzheimer's disease. *Nature*. 2018;560(7717):185-191. doi:10.1038/s41586-018-0368-8
- Scheltens P, De Strooper B, Kivipelto M, et al. Alzheimer's disease. *Lancet*. 2021;397(10284):1577-1590. doi:10.1016/S0140-6736(20)32205-4
- Collaborators GBDD. Global, regional, and national burden of Alzheimer's disease and other dementias, 1990-2016: a systematic analysis for the Global Burden of Disease Study 2016. *Lancet Neurol*. 2019;18(1):88-106. doi:10.1016/S1474-4422(18)30403-4
- Jack CR Jr, Thorneau TM, Weigand SD, et al. Prevalence of biologically vs clinically defined Alzheimer spectrum entities using the National Institute on Aging-Alzheimer's Association Research Framework. *JAMA Neurol*. 2019;76(10):1174-1183. doi:10.1001/jamaneurol.2019.1971
- Scheltens NM, Galindo-Garre F, Pijnenburg YA, et al. The identification of cognitive subtypes in Alzheimer's disease dementia using latent class analysis. *J Neurol Neurosurg Psychiatry*. 2016;87(3):235-243. doi:10.1136/jnnp-2014-309582
- Taylor X, Clark IM, Fitzgerald GJ, et al. Amyloid-beta (A β) immunotherapy induced microhemorrhages are associated with activated perivascular macrophages and peripheral monocyte

- recruitment in Alzheimer's disease mice. *Mol Neurodegener.* 2023;18(1):59. doi:10.1186/s13024-023-00649-w
21. Adhikari UK, Khan R, Mikhael M, et al. Therapeutic anti-amyloid beta antibodies cause neuronal disturbances. *Alzheimers Dement.* 2023;19(6):2479-2496. doi:10.1002/alz.12833
 22. Joseph-Mathurin N, Dorieux O, Trouche SG, et al. Amyloid beta immunization worsens iron deposits in the choroid plexus and cerebral microbleeds. *Neurobiol Aging.* 2013;34(11):2613-2622. doi:10.1016/j.neurobiolaging.2013.05.013
 23. Pan R-Y, Zhang J, Wang J, et al. Intermittent fasting protects against Alzheimer's disease in mice by altering metabolism through remodeling of the gut microbiota. *Nature Aging.* 2022;2(11):1024-1039. doi:10.1038/s43587-022-00311-y
 24. Pitts MW. Barnes maze procedure for spatial learning and memory in Mice. *Bio Protoc.* 2018;8(5). doi:10.21769/bioprotoc.2744
 25. Zhang Y, Xu J, Ruan YC, et al. Implant-derived magnesium induces local neuronal production of CGRP to improve bone-fracture healing in rats. *Nat Med.* 2016;22(10):1160-1169. doi:10.1038/nm.4162
 26. Feng X, Frias ES, Paladini MS, et al. Functional role of brain-grafted macrophages against brain injuries. *J Neuroinflammation.* 2021;18(1):232. doi:10.1186/s12974-021-02290-0
 27. Dukhinova M, Veremeyko T, Yung AWY, et al. Fresh evidence for major brain gangliosides as a target for the treatment of Alzheimer's disease. *Neurobiol Aging.* 2019;77:128-143. doi:10.1016/j.neurobiolaging.2019.01.020
 28. Louveau A, Filiano AJ, Kipnis J. Meningeal whole mount preparation and characterization of neural cells by flow cytometry. *Curr Protoc Immunol.* 2018;121(1):e50. doi:10.1002/cpim.50
 29. Lu X, Chen L, Jiang C, Cao K, Gao Z, Wang Y. Microglia and macrophages contribute to the development and maintenance of sciatica in lumbar disc herniation. *Pain.* 2023;164(2):362-374. doi:10.1097/j.pain.0000000000002708
 30. da Huang W, Sherman BT, Lempicki RA. Bioinformatics enrichment tools: paths toward the comprehensive functional analysis of large gene lists. *Nucleic Acids Res.* 2009;37(1):1-13. doi:10.1093/nar/gkn923
 31. da Huang W, Sherman BT, Lempicki RA. Systematic and integrative analysis of large gene lists using DAVID bioinformatics resources. *Nat Protoc.* 2009;4(1):44-57. doi:10.1038/nprot.2008.211
 32. Babicki S, Arndt D, Marcu A, et al. Heatmapper: web-enabled heat mapping for all. *Nucleic Acids Res.* 2016;44(W1):W147-53. doi:10.1093/nar/gkw419
 33. Carpentier G, Berndt S, Ferratge S, et al. Angiogenesis analyzer for ImageJ—a comparative morphometric analysis of "Endothelial Tube Formation Assay" and "Fibrin Bead Assay". *Sci Rep.* 2020;10(1):11568. doi:10.1038/s41598-020-67289-8
 34. Ahn JH, Cho H, Kim JH, et al. Meningeal lymphatic vessels at the skull base drain cerebrospinal fluid. *Nature.* 2019;572(7767):62-66. doi:10.1038/s41586-019-1419-5
 35. Da Mesquita S, Papadopoulos Z, Dykstra T, et al. Meningeal lymphatics affect microglia responses and anti-Abeta immunotherapy. *Nature.* 2021;593(7858):255-260. doi:10.1038/s41586-021-03489-0
 36. Louveau A, Da Mesquita S, Kipnis J. Lymphatics in Neurological disorders: a neuro-lympho-vascular component of multiple sclerosis and Alzheimer's disease? *Neuron.* 2016;91(5):957-973. doi:10.1016/j.neuron.2016.08.027
 37. Jiang-Xie LF, Drieu A, Kipnis J. Waste clearance shapes aging brain health. *Neuron.* 2024. doi:10.1016/j.neuron.2024.09.017
 38. Secker GA, Harvey NL. Regulation of VEGFR signalling in lymphatic vascular development and disease: an update. *Int J Mol Sci.* 2021;22(14):7760. doi:10.3390/ijms22147760
 39. Cugurra A, Mamuladze T, Rustenhoven J, et al. Skull and vertebral bone marrow are myeloid cell reservoirs for the meninges and CNS parenchyma. *Science.* 2021;373(6553):eabf7844. doi:10.1126/science.abf7844
 40. Meizlish ML, Kimura Y, Pope SD, et al. Mechanosensing regulates tissue repair program in macrophages. *Sci Adv.* 2024;10(11):eadk6906. doi:10.1126/sciadv.adk6906
 41. Shimada R, Tatara Y, Kibayashi K. Gene expression in meningeal lymphatic endothelial cells following traumatic brain injury in mice. *PLoS One.* 2022;17(9):e0273892. doi:10.1371/journal.pone.0273892
 42. Biswas L, Chen J, De Angelis J, et al. Lymphatic vessels in bone support regeneration after injury. *Cell.* 2023;186(2):382-397 e24. doi:10.1016/j.cell.2022.12.031
 43. Apaydin A, Yazdirduyev B, Can T, Keklikoglu N. Soft tissue changes during distraction osteogenesis. *Int J Oral Maxillofac Surg.* 2011;40(4):408-412. doi:10.1016/j.ijom.2010.11.007
 44. Mackool RJ, Hopper RA, Grayson BH, Holliday R, McCarthy JG. Volumetric change of the medial pterygoid following distraction osteogenesis of the mandible: an example of the associated soft-tissue changes. *Plast Reconstr Surg.* 2003;111(6):1804-1807. doi:10.1097/01.PRS.0000055431.19215.OA
 45. Rowe NM, Mehrara BJ, Luchs JS, et al. Angiogenesis during mandibular distraction osteogenesis. *Ann Plast Surg.* 1999;42(5):470-475. doi:10.1097/0000637-199905000-00002
 46. Hauglund NL, Kusk P, Kornum BR, Nedergaard M. Meningeal lymphangiogenesis and enhanced glymphatic activity in mice with chronically implanted EEG electrodes. *J Neurosci.* 2020;40(11):2371-2380. doi:10.1523/JNEUROSCI.2223-19.2020
 47. Dai W, Yang M, Xia P, et al. A functional role of meningeal lymphatics in sex difference of stress susceptibility in mice. *Nat Commun.* 2022;13(1):4825. doi:10.1038/s41467-022-32556-x
 48. Song E, Mao T, Dong H, et al. VEGF-C-driven lymphatic drainage enables immunosurveillance of brain tumours. *Nature.* 2020;577(7792):689-694. doi:10.1038/s41586-019-1912-x
 49. Keiser MS, Ranum PT, Yrigollen CM, et al. Toxicity after AAV delivery of RNAi expression constructs into nonhuman primate brain. *Nat Med.* 2021;27(11):1982-1989. doi:10.1038/s41591-021-01522-3
 50. Secker GA, Harvey NL. VEGFR signaling during lymphatic vascular development: from progenitor cells to functional vessels. *Dev Dyn.* 2015;244(3):323-331. doi:10.1002/dvdy.24227
 51. Laaker C, Fabry Z. The meningeal lymphatics: regulators of Abeta immunotherapy?. *Trends Immunol.* 2021;42(11):940-942. doi:10.1016/j.it.2021.09.011
 52. Liao S, von der Weid PY. Inflammation-induced lymphangiogenesis and lymphatic dysfunction. *Angiogenesis.* 2014;17(2):325-334. doi:10.1007/s10456-014-9416-7
 53. Huang YH, Yang HY, Huang SW, Ou G, Hsu YF, Hsu MJ. Interleukin-6 induces vascular endothelial growth factor-C expression via Src-FAK-STAT3 signaling in lymphatic endothelial cells. *PLoS One.* 2016;11(7):e0158839. doi:10.1371/journal.pone.0158839
 54. Shi C, Pamer EG. Monocyte recruitment during infection and inflammation. *Nat Rev Immunol.* 2011;11(11):762-774. doi:10.1038/nri3070
 55. Angeli V, Ginhoux F, Llodra J, et al. B cell-driven lymphangiogenesis in inflamed lymph nodes enhances dendritic cell mobilization. *Immunity.* 2006;24(2):203-215. doi:10.1016/j.immuni.2006.01.003
 56. Planas-Paz L, Strilic B, Goedecke A, Breier G, Fassler R, Lammert E. Mechanoinduction of lymph vessel expansion. *EMBO J.* 2012;31(4):788-804. doi:10.1038/emboj.2011.456
 57. Louveau A, Herz J, Alme MN, et al. CNS lymphatic drainage and neuroinflammation are regulated by meningeal lymphatic vasculature. *Nat Neurosci.* 2018;21(10):1380-1391. doi:10.1038/s41593-018-0227-9
 58. Hsu M, Rayasam A, Kijak JA, et al. Neuroinflammation-induced lymphangiogenesis near the cribriform plate contributes to drainage of CNS-derived antigens and immune cells. *Nat Commun.* 2019;10(1):229. doi:10.1038/s41467-018-08163-0
 59. Li X, Qi L, Yang D, et al. Meningeal lymphatic vessels mediate neurotropic viral drainage from the central nervous system. *Nat Neurosci.* 2022;25(5):577-587. doi:10.1038/s41593-022-01063-z

60. Salvador AFM, Dykstra T, Rustenhoven J, et al. Age-dependent immune and lymphatic responses after spinal cord injury. *Neuron*. 2023;111(14):2155-2169.e9. doi:[10.1016/j.neuron.2023.04.011](https://doi.org/10.1016/j.neuron.2023.04.011)
61. Mrdjen D, Pavlovic A, Hartmann FJ, et al. High-dimensional single-cell mapping of central nervous system immune cells reveals distinct myeloid subsets in health, aging, and disease. *Immunity*. 2018;48(2):380-395.e6. doi:[10.1016/j.immuni.2018.01.011](https://doi.org/10.1016/j.immuni.2018.01.011)
62. Antila S, Karaman S, Nurmi H, et al. Development and plasticity of meningeal lymphatic vessels. *J Exp Med*. 2017;214(12):3645-3667. doi:[10.1084/jem.20170391](https://doi.org/10.1084/jem.20170391)
63. Makinen T, Jussila L, Veikkola T, et al. Inhibition of lymphangiogenesis with resulting lymphedema in transgenic mice expressing soluble VEGF receptor-3. *Nat Med*. 2001;7(2):199-205. doi:[10.1038/84651](https://doi.org/10.1038/84651)
64. Yanev P, Poinatte K, Hominick D, et al. Impaired meningeal lymphatic vessel development worsens stroke outcome. *J Cereb Blood Flow Metab*. 2020;40(2):263-275. doi:[10.1177/0271678X18822921](https://doi.org/10.1177/0271678X18822921)
65. Ma Q, Ineichen BV, Detmar M, Proulx ST. Outflow of cerebrospinal fluid is predominantly through lymphatic vessels and is reduced

in aged mice. *Nat Commun*. 2017;8:1434. doi:[10.1038/s41467-017-01484-6](https://doi.org/10.1038/s41467-017-01484-6)

SUPPORTING INFORMATION

Additional supporting information can be found online in the Supporting Information section at the end of this article.

How to cite this article: Lu X, Bai S, Feng L, et al. Cranial bone maneuver ameliorates Alzheimer's disease pathology via enhancing meningeal lymphatic drainage function. *Alzheimer's Dement*. 2025;21:e14518. <https://doi.org/10.1002/alz.14518>